POLITECNICO
MILANO 1863

SCUOLA DI INGEGNERIA INDUSTRIALE
E DELL'INFORMAZIONE

Time, amplitude, and frequency dependence of the Payne effect a study on silica-filled styrene-butadiene rubbers

MASTER THESIS IN
MATERIALS ENGINEERING AND NANOTECHNOLOGY
INGEGNERIA DEI MATERIALI E DELLE NANOTECNOLOGIE

Author: **Jacopo Cervi**

Student ID: 977627
Advisor: F. Briatico Vangosa
Co-advisor: C. Marano
Academic Year: 2022-23

Abstract

This research explores the influence of strain amplitude on the nonlinear viscoelastic behavior of silica-filled styrene-butadiene and acrylonitrile-butadiene rubbers, a phenomenon known as the Payne effect. The study delves into the time-dependent aspects to assess the reversible nature of structural changes caused by strain amplitude. Experimental tests have been carried out using the torsional Dynamic Mechanical Analysis technique with a prismatic specimen's configuration. Experiments, conducted at ambient temperature with variable frequencies, involved oscillatory sinusoidal tests under controlled shear strain. The inherent nonlinearities in these materials limit the applicability of traditional viscoelastic theories in oscillatory experiments for property assessment. To address this, an initial evaluation using FT-rheology focused on higher harmonics, showed that the level of nonlinearity is limited to an extent that the classical interpretation of material properties via storage (G') and loss (G'') moduli is acceptable. Furthermore, the study investigates the frequency's impact on this complex nonlinear response, particularly examining the purported frequency-insensitivity of the Payne effect.

Finally, using appropriate oscillating strain histories it was possible to demonstrate the full reversibility of the structural changes involved in the Payne effect for the filled rubber considered in this work.

Key-words: Payne effect, reinforced elastomers, reversibility, recovery, frequency effect

Abstract in italiano

Questa ricerca esplora l'influenza dell'ampiezza di sforzo sul comportamento viscoelastico non lineare di gomme rinforzate con silice, come le gomme stirene-butadiene e l'acrilonitrile-butadiene, un fenomeno noto come effetto Payne. Lo studio si addentra negli aspetti dipendenti dal tempo per valutare la natura reversibile dei cambiamenti strutturali causati dall'ampiezza della deformazione. Sono stati effettuati test sperimentali utilizzando la tecnica di Analisi Dinamico Meccanica in torsione con una configurazione prismatica del campione. Gli esperimenti, condotti a temperatura ambiente con frequenze variabili, sono stati svolti in oscillazione sinusoidale controllando la deformazione a taglio. Le non linearità intrinseche in questi materiali limitano l'applicabilità delle teorie viscoelastiche tradizionali negli esperimenti oscillatori per la valutazione delle proprietà. Per affrontare ciò, una valutazione iniziale utilizzando la FT-reologia si è concentrata sugli armonici superiori, ha mostrato che il livello di non-linearità è limitato a tal punto che l'interpretazione classica delle proprietà del materiale tramite i moduli di conservazione (G') e perdita (G'') è accettabile. Inoltre, lo studio indaga l'impatto della frequenza su questa complessa risposta non lineare, esaminando in particolare la presunta insensibilità alla frequenza dell'effetto Payne.

Infine, utilizzando storie di deformazione oscillante appropriate, è stato possibile dimostrare la completa reversibilità dei cambiamenti strutturali coinvolti nell'effetto Payne per la gomma riempita considerata in questo lavoro.

Parole chiave: Effetto Payne, elastomeri rinforzati, reversibilità, recupero, effetto della frequenza

Contents

Introduction

Numerous applications including tires, damping devices, and belts for transmitting power utilize reinforced rubbers. These are typically vulcanized elastomers strengthened by inorganic particles like carbon black and silica. This thesis addresses the complex behavior of reinforced rubbers, display complex behavior due to their nonlinear reaction to increasing amplitudes in oscillating strains. This phenomenon, identified in the 1960s, describes the softening of the storage modulus component in filled rubbers with varying strain amplitudes, it is the so-called Payne effect.

The focus of this study is the nonlinear relationship between the shear dynamic modulus components and strain amplitude in torsional oscillatory experiments on styrene-butadiene rubber (SBR) and acrylonitrile-butadiene rubber (NBR) with different silica contents. Employing the simple and practical torsional setup on the Anton Paar MRC502-rheometer using rectangular specimens, the research starts with an analysis of shear stress responses from amplitude sweep experiments to quantify the higher harmonics. The not significant presence of higher harmonics results in supporting the use of the linear viscoelastic theory to elaborate and represent data in terms of storage and loss components of the dynamic modulus.

The study of materials containing varying amounts of filler aligns with existing literature findings: the inclusion of particles significantly changes the viscoelastic response, compared to the properties of unfilled rubber. Specifically, reinforced rubbers exhibit a non-linear viscoelastic behavior when the shear strain amplitude approaches approximately 0.5%, in contrast to unfilled rubber, which maintains a linear viscoelastic behavior up to 30%.

A crucial aspect of this thesis has been demonstrating the reversible nature of structural changes induced by the Payne effect, because a comprehensive understanding of this aspect is lacking in literature. This study bridges this knowledge gap by conducting detailed experiments to observe and analyze these changes, through the monitoring of the properties over a large range of time scales.

Additionally, this thesis research investigates how frequency influences the dynamic modulus's nonlinear dependency on amplitude. This work further explores these aspects in order to assess the separability of frequency and amplitude variables which prior studies have noted in the dynamic modulus analysis.

In summary, this thesis aims to deepen the understanding of the Payne effect in reinforced rubbers by examining their nonlinear viscoelastic behavior under

oscillatory strain. Through theoretical and experimental methods, the study contributes to the broader knowledge of this critical phenomenon in material science, with potential implications for its practical applications.

1 Theoretical background

The subsequent sections provide an in-depth description of the structure and behaviour of elastomers, together with an exploration of the governing principles of viscoelastic materials as characterized by Dynamic Mechanical Analysis (DMA). Attention then shifts to the distinctive nonlinear behaviour observed in filler-reinforced elastomers and referred to as Payne effect when linearity is described in terms of dependence of dynamic mechanical properties on strain amplitude. This includes a comprehensive examination of various interpretations of the Payne effect, culminating in an analysis of the unique phenomena and specific dependencies inherent in this nonlinear effect.

1.1. Elastomers

1.1.1. General description of elastomers

Elastomers, commonly referred to as rubber, hold a central position in an array of industrial applications, primarily due to their exceptional physical attributes. To truly appreciate the outstanding characteristics of elastomers, it is essential to delve into their intricate internal structure. [1]

At the core of elastomers lies a distinctive internal arrangement, characterized by long, flexible chain-like molecules that intertwine and form entanglements [1] [2]. These macromolecular chains exhibit a remarkable degree of flexibility and mobility, constantly undergoing conformational changes due to thermal agitation [1] [2]. In fact, the defining feature of elastomers lies in their extraordinary capacity to undergo substantial deformations [2].

Before their deployment in industrial applications, elastomers often undergo physical and chemical treatments aimed at enhancing their mechanical properties. One of the most significant processes in this regard is vulcanization, which involves the chemical creation of covalent network junctions through the insertion of crosslinks between polymer chains. Typically, vulcanization involves heating the rubber, combined with sulfur-based vulcanizing agents, within a mold under pressure [2] [3]. It is worth noting that some linkages between chains may be physical and thermo-reversible, granting a temporary character to the network structure [2].

The resulting network structure imparts elastomers with solid-like characteristics, significantly increasing their elasticity while decreasing their plasticity. Under external stresses, these chain networks inhibit relative motions, allowing rubber to stretch up to approximately ten times its original length. Upon the removal of external forces, the material rapidly reverts to its initial dimensions, exhibiting virtually no residual or non-recoverable strain [2].

Furthermore, this network formation renders rubber practically insoluble in solvents and furthermore renders it unsuitable for processing methods involving flow, such as mixing, extrusion, milling, or molding. Consequently, vulcanization must occur only after the rubber article assumes its final geometric form [2]. This intricate interplay between molecular structure and processing techniques consolidates the unique elasticity and functionality of elastomers, setting the stage for a deeper exploration into the material's specifics.

1.1.2. Elasticity of elastomers

Understanding the remarkable elasticity displayed by elastomers requires a closer examination of the underlying mechanisms governing their behavior. Elastomeric chains exhibit a collection of conformations influenced by three key factors: the statistical nature of random processes, preferences for specific bond arrangements driven by steric and energetic constraints within the molecule, and the exclusion of hypothetical conformations necessitating overlapping chain segments in space [2].

Notably, the tension experienced by elastomers primarily arises from an entropic mechanism. It originates from the inherent tendency of the polymer chains to adopt configurations characterized by maximum randomness, rather than any energetic preference for one conformation over another [2]. This entropic effect lies at the heart of their singular elasticity.

In rubber elasticity, macroscopic deformation primarily induces conformational transitions in the polymer. Initially in a compact, disordered, random coil state, the chains gradually align in the direction of the applied strain. Significant elongation stresses bond lengths and angles, affecting internal energy. This deformation reduces the system's disorder, leading to a decrease in entropy (loss of conformational freedom). The driving force to elastic recovery is entropic, as the material seeks to return to a state of minimum free energy by increasing entropy. Notably, in the absence of crosslinking, a stretched rubber can spontaneously revert to its high entropy state (random coil) through viscous flow and thermal motions [4].

In contrast, vulcanized elastomers respond differently to external traction. The molecular chains align parallel to the macro-displacement due to the presence of crosslinks introduced during vulcanization. These crosslinks prevent the chains from returning to their initial disordered state, imparting greater stability to the material. It's worth highlighting that the formation of crosslinks significantly reduces hysteresis,

which is the ratio of the viscous component to the elastic component of deformation resistance [2].

The behavior of both vulcanized and non-vulcanized rubber specimens under a tensile load is highlighted in Figure 1.1.

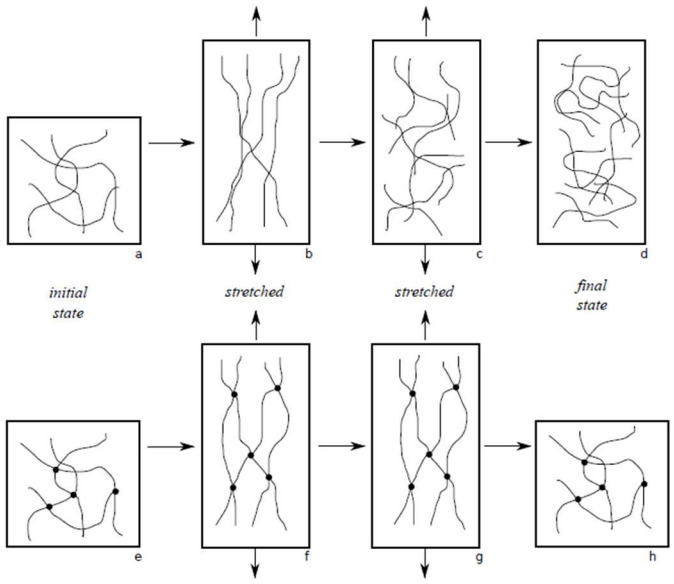

Figure 1.1. Effect of stretching on a non-vulcanized (above) and a vulcanized (below) elastomer.

In conclusion, these insights into the entropic nature of elastomers' elasticity underscore the fundamental principles driving their behavior. This knowledge forms the basis for our in-depth exploration of "Filled elastomers" in the upcoming section.

1.2. Reinforced elastomers

The enhancement of elastomers through the incorporation of particulate fillers has been a subject of extensive investigation, particularly during the 1960s and 1970s. The motivation for this exploration derives from two distinct yet connected factors. Firstly, the profound alterations in mechanical properties induced by filler reinforcement have rendered many applications of elastomers possible. Secondly, the enigmatic nature of the reinforcement mechanism has captivated scientists, and despite persistent efforts, it remains largely uncharted territory today [2].

In contrast to plastics, where reinforcement leads to an increase in modulus and hardness, but on the other hand the deformation at break decreases, elastomers exhibit a unique response. When reinforcing fillers are introduced, elastomers experience a simultaneous increase in modulus and deformation at break, a phenomenon at odds with traditional expectations. This intriguing paradox, although not entirely comprehended, underscores the distinctive ability of reinforced elastomers to offer

exceptional material properties and applications. It also justifies their widespread success across various technological domains [2].

Elastomers benefit from a variety of fillers, including carbon black, silica, and newer reinforcing agents [2].

In the 1960s, the interaction between carbon black and elastomers was initially attributed to chemical bonding [5] [6]. Silica-reinforced blends, in contrast, initially displayed lower mechanical properties, especially concerning stress at break and abrasion resistance. However, two significant breakthroughs paved the way for silicas to achieve properties like carbon black mixes. The first, in the 1970s, was the introduction of specific coupling agents by Wolff [7] [8]. The second, in the 1990s, was proposed by Rauline, involving the utilization of specific precipitation silica, elastomers, and tailored mixing conditions to achieve effective reinforcement [9].

Additionally, numerous reinforcing systems have been patented, encompassing alumina oxyhydroxide, oxides, titanium oxides, and silicon nitride/carbide [10] [11] [12] [13] [14].

Morphology and physicochemical properties of reinforcing fillers are of crucial importance as they directly define their reinforcement ability. Consequently, their characterization is fundamental and primarily relies on morphological properties (sizes, surface area, and structure), dispersibility, and surface chemistry [2].

1.2.1. Fillers-elastomers interactions

The interactions between fillers and elastomers are essential in understanding the reinforcement mechanisms that are responsible for the mechanical properties of filled elastomers, a topic we delve into in this section.

Carbon Black:

- *Filler Network* - Carbon black's high surface energy exerts a substantial influence on elastomeric chains. These chains become strongly adsorbed onto the carbon black surface, leading to a significant reduction in their mobility, especially in regions referred to as "trains" [15] [16] [17] [18]. A more refined perspective recognizes that elastomeric chains exhibit a gradient of mobility, ranging from the carbon black surface to the bulk of the material. The bonding of carbon black aggregates gives rise to the formation of a filler network [2]. This network emerges due to the statistical size of polymeric chains, which falls within the range of interaggregate distances. The high surface areas and loadings of carbon blacks used in elastomer reinforcement further induce proximity between reinforcing objects, resulting in elastomeric chains interacting with multiple aggregates, potentially binding neighboring objects together [19].

- *Chemical Surface Bonding* - Strong links keep the chains attached to the filler surface hence, following Medalia and Kraus [20], chemical reactions could occur at the carbon black matrix interface.

Silica:

In contrast to carbon black, achieving silica elastomer reinforcement typically requires the use of a coupling agent. TESPT, a silane-based compound, is widely employed as a coupling agent due to its bifunctionality, enabling the formation of covalent bonds between silica surfaces and elastomeric chains [2].

- *Polymer Adsorption* - Polymer adsorption naturally occurs [21] [22], but the presence of the coupling agent limits this process due to its shielding effect. Consequently, in silica-silane-elastomer compounds, the filler network is generally less extended than in carbon black-elastomer systems. Despite this, the reduction in elastomeric chain mobility near the silica surface follows a similar qualitative trend [23]. Due to the high polarity of silica, direct interactions between silica aggregates may also occur, forming an additional filler-filler network. However, the extent of the filler network is contingent on the amount of coupling agent used [2].

Recently, Huang et all. [24] introduced an advanced model that details the interactions between silica fillers and rubber matrices. In this study of uncured rubber mixed with silica, the model categorizes the elastomeric chains into four distinct states: tightly bound rubber, loosely bound rubber, free rubber, and entrapped rubber. The last category, "entrapped rubber," refers to elastomeric molecules enveloped within the filler network. The distinctions and specifics of these chain states are effectively illustrated in the accompanying figure.

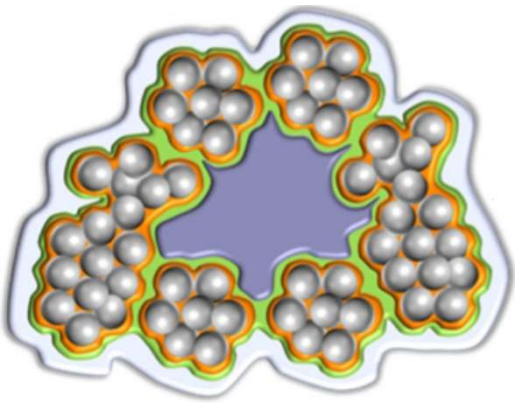

Figure 1.2: Representation of the model introduced by Huang et all. (2023)

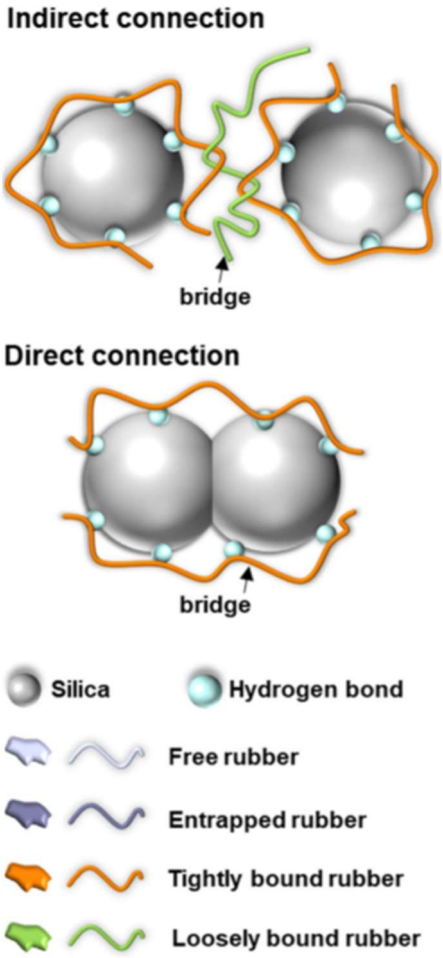

Figure 1.3. Description of the model introduced by Huang et all. (2023)

The introduction of fillers significantly modifies various mechanical properties due to the complex interactions discussed earlier. Qualitatively, attributes like strength, tear and abrasion resistance, as well as stiffness, experience substantial improvements compared to the neat elastomer. The inclusion of fillers also has a profound impact on the material's dissipative behavior and temperature sensitivity [2].

It's important to note that the complex interplay of these interactions introduces nonlinear behaviors to certain material responses. Two notable nonlinear phenomena extensively studied in the literature are the Mullins effect, which pertains to quasi-static behavior, and the Payne effect, which relates to dynamic responses [1]. These nonlinearities add depth and intricacy to the understanding of filled elastomers' mechanical properties, enhancing their utility in various applications.

To facilitate an in-depth discussion of this nonlinear dynamic response known as the Payne effect, it is essential to initially undertake a concise review of the theoretical foundations around dynamic mechanical analysis (DMA).

To be more precise, the Mullins effect is observed during repeated loading-unloading cycles, as depicted in Figure 1.4. Typically, a gradual softening in the loading curves occurs over these cycles, potentially leading to residual deformation. This effect is linked to the rearrangement of labile bonds, but it can also result from mechanical degradation when these cycles involve extremely high elongations [4].

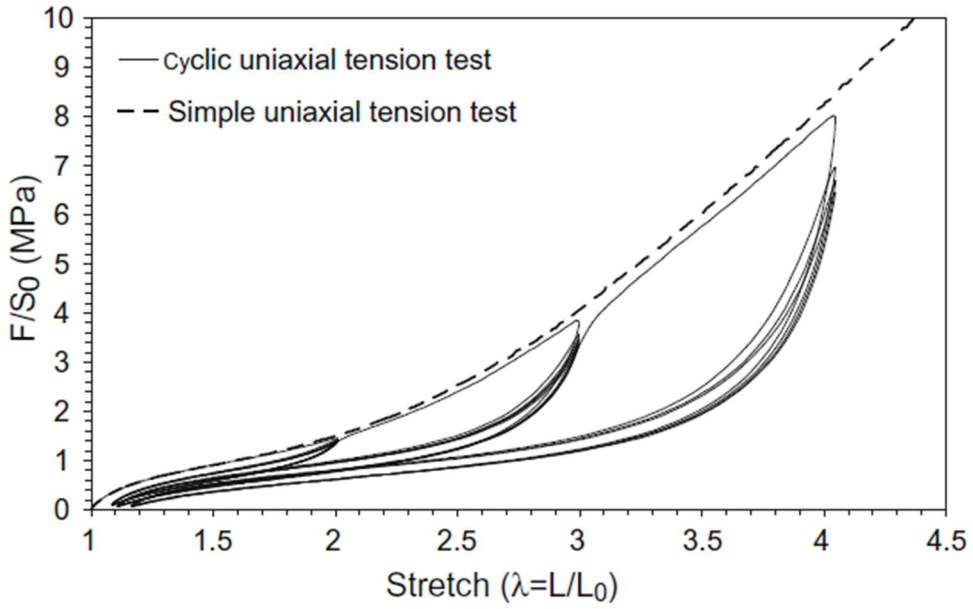

Figure 1.4. Stress-strain responses of a 50 phr carbon-black filled SBR submitted to a simple uniaxial tension and to a cyclic uniaxial tension with increasing maximum stretch every 5 cycles [25]

1.3. Dynamic mechanical analysis

Dynamic Mechanical Analysis (DMA) is instrumental in elucidating the viscoelastic behavior of polymers, particularly due to its capability to analyze the material's time-dependent response in terms of dependency on frequency when subjected to sinusoidal inputs in steady state.

At the heart of DMA is the measurement of a material's steady-state response to a sinusoidal strain or stress at a constant frequency. For instance, applying a sinusoidal shear strain can be mathematically expressed as:

$$\gamma(t) = \gamma_0 \sin(\omega t) \qquad 1.1$$

where γ_0 denotes the strain amplitude, ω the angular frequency and t the time.

A perfectly elastic response (also called solid-like), following Hooke's law (Equation 1.2), would occur without phase delay in relation to the strain. In contrast, the liquid-

like response follows the Newton's law (Equation 1.3), therefore it would be in phase with the strain rate, exhibits a phase delay of $\pi/2$ with respect to the sinusoidal strain.

$$\tau = G\gamma \tag{1.2}$$

$$\tau = \eta \frac{d\gamma}{dt} \tag{1.3}$$

For materials displaying linear viscoelastic properties, the shear stress τ oscillates sinusoidally as well, but with a phase angle δ between 0 and $\pi/2$. This angle indicates the phase shift between stress and strain. Mathematically, the stress response can be divided into two components: τ' and τ'', representing the in-phase, elastic and in quadrature, viscous responses, respectively. The elastic stress component τ', in phase with the strain, represents the material's ability to store energy elastically. In contrast, the viscous component τ'', with $\delta = \pi/2$, indicates the material's capacity to dissipate energy.

These stress components help define material properties. The elastic modulus G', or storage modulus, is the ratio of the elastic stress component amplitude to the strain amplitude, given by:

$$G'(\omega) = \frac{\tau_0 \cos(\delta)}{\gamma_0} \tag{1.4}$$

The viscous, or loss, modulus G'' is calculated from the ratio of the viscous stress component amplitude to the strain, indicating the material's propensity for energy dissipation, as shown in:

$$G''(\omega) = \frac{\tau_0 \sin(\delta)}{\gamma_0} \tag{1.5}$$

The complex modulus G^* integrates both elastic and viscous elements, representing the overall deformation resistance.

$$G^*(\omega) = G'(\omega) + iG''(\omega) \tag{1.6}$$

The ratio of G'' to G' (Equation 1.7), provides insights into the damping characteristics of the material, crucial for understanding polymer behavior under cyclic loading.

$$\tan(\delta(\omega)) = \frac{G'(\omega)}{G''(\omega)} \tag{1.7}$$

It's important to note that these relationships are primarily established in shear stress/strain state, where the relevant modulus is G, while in uniaxial tensile state, E denotes the appropriate property.

All information explained above are referred to [26], [27] and [2].

1.3.1. Rectangular geometry torsion

In the exploration of shear deformations, a variety of experimental setups have been utilized. Particularly, Sternstein et al. (2000) and Rizza (2020) [28] [29] used a shear sandwich tool, while Li (2017) and other authors [30] [31] [32] applied parallel plates in rotation. The relatively new technology RPA is used by Randall at al. 2014 [33]. In this experimental work, our focus is on a torsional geometry tool (Figure 1.5) to study deformations in rectangular specimens.

Figure 1.5. Torsional rectangular geometry tool

Addressing the in-plane shear stress distribution in rectangular specimens is complex [34]. When torque is applied to such specimens, the resulting stress field includes two torsion components: primary and secondary. The primary torsion solution, commonly adopted in commercial rheometers, operates under the assumption that sections perpendicular to the rotational axis are free to warp. This, however, is an oversimplification, given that the specimen ends are clamped, restricting warping [35]. Thus, secondary torsion, or warping torsion, comes into play. It arises from tangential stresses that counterbalance the normal stresses caused by these clamping-induced constraints. This interaction misleadingly increases the torsional stiffness, leading to an overestimation in the measured shear modulus, especially in less slender specimens.

Considering these intricacies, the selection of prismatic specimen sizes becomes crucial. Luca Di Giosia's (2022) [36] extensive research in this area has been quite useful on determining the optimal geometry, and its results are applied in this experimental work.

1.4. Payne effect

1.4.1. Description of the Payne effect

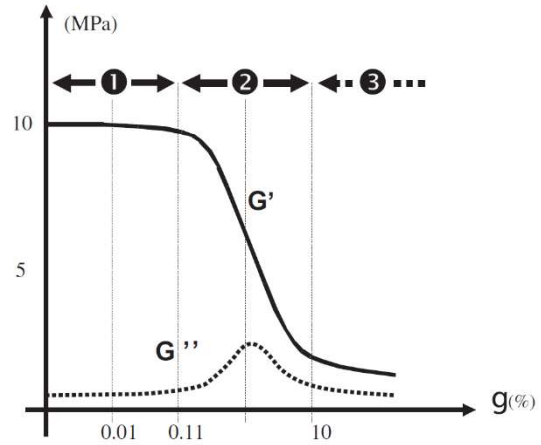

Figure 1.6. Schematic illustration G' and G'' variation divided in three strain amplitude zones

The Payne effect, crucial in the study of filled rubbers, was first documented by Fletcher and Gent (1953) [37] and further elaborated by Payne (1962) [38]. This phenomenon describes the non-linear softening behavior of rubber materials under oscillatory displacement, observed as a strong dependence of the dynamic stress response on the applied strain amplitude. This characteristic behavior forms a key aspect of the viscoelastic properties of filled rubbers, which are essential components in many practical applications, including automobile tires, damping devices, and power transmission belts. The significance of the Payne effect in such applications arises from the typical dynamic stresses and strains these materials are subjected on, directly correlating with the effect's parameters [39] [30].

Despite extensive research, the fundamental nature of the Payne effect and the underlying mechanisms remain partially unresolved. Over a hundred publications have focused on various aspects of this phenomenon, enriching the field but also highlighting the complexity surrounding it [39]. Chazeau et al. (2000) [29] notably classified mechanism-based models that seek to explain the Payne effect, contributing significantly to our understanding.

One explanatory model is Dannenberg's molecular slippage model (1996) [40], which delves into the interaction between elastomer chains and filler particles. Initially, these chains are adsorbed onto the filler surface. At low strain amplitude (Figure 1.6 - Figure 1.7), the chains extend, storing the deformation energy as elastic energy, which is recoverable upon strain reduction, resulting in a low and constant loss modulus G''.

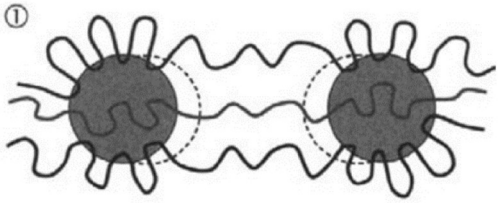

Figure 1.7. Chains stretching at low strain amplitude Zone 1

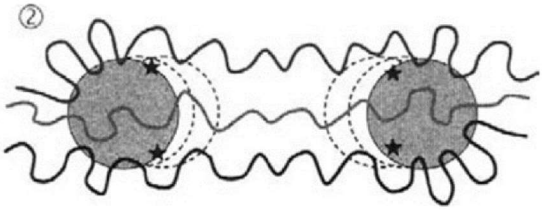

Figure 1.8. Chains desorption at medium strain amplitude Zone 2

As strain progresses (Figure 1.6 and Figure 1.8), the stored elastic energy surpasses the adsorption energy, causing elastomer chains to gradually desorb from the filler surface. This desorption is a gradual process, influenced by a broad distribution of interaggregate distances, leading to various lengths of bridging elastomer segments. Dannenberg suggests that eventually, this gradual desorption, which results in homogenization of segment lengths, explains the stabilization of the modulus in the Payne effect's third zone. Thus, the Payne effect not only highlights the unique viscoelastic properties of filled rubbers but also provides insight into the molecular dynamics governing rubber-filler interactions.

1.4.2. Linear-nonlinear dichotomy

In the field of dynamic mechanical analysis (DMA), understanding the behavior of materials under oscillatory strain is essential. At small strain amplitudes, the material's response is linear and characterized by the viscoelastic moduli G' and G'' [41]. However, as strain amplitude is increased, the response enters a nonlinear viscoelastic regime, and the decomposition in an elastic and viscous component is inadequate, given the appearance on higher order harmonics in the stress periodic response.

To quantify the behavior under large amplitude oscillatory strain (LAOS), Fourier transform (FT) rheology is commonly employed [42]. This approach involves representing the stress response to sinusoidal strain input through a Fourier series [43]. In the linear regime, this response will mainly contain the first harmonic ($n = 1$), i.e. an out of phase sinusoid. However, with increased strain, nonlinear responses emerge, marked by the growth of higher harmonic contributions. Although mathematically sound, FT rheology has limitations, such as sensitivity to nonlinearity without providing a clear physical interpretation of higher-order coefficients [44].

Addressing these challenges, Ewoldt (2008) [44] introduced new metrics for analyzing nonlinearities in LAOS tests, offering the advantage of a clearer physical interpretation. However, there remain some fundamental questions concerning Ewoldt's approach as discussed by Rogers et al. (2018) [45].

An intriguing aspect of the Payne effect, particularly in vulcanized rubber compounds, is that despite the reduction of modulus with increasing strain common to many soft materials [46] [47] [48], the response to forced oscillatory shear remains almost sinusoidal, distinctly lacking higher order harmonics across all considered strain amplitudes (Figure 1.9) [39] [29] [49] [33] [50]. This peculiar behavior, termed "The linear-nonlinear dichotomy" by Roberson et al. (2006) [39], is a key characteristic differentiating the Payne effect from other types of viscoelastic nonlinearity. This absence of higher harmonics in filled rubber is evident when examining the ratio of Fourier coefficients: third harmonic response relative to the first (Figure 1.10).

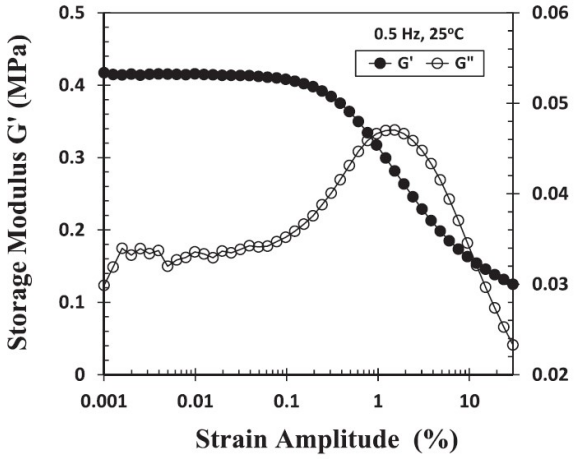

Figure 1.9. Dependence of G' and G'' on strain amplitude. The test material: SBR-CR rubber. [30]

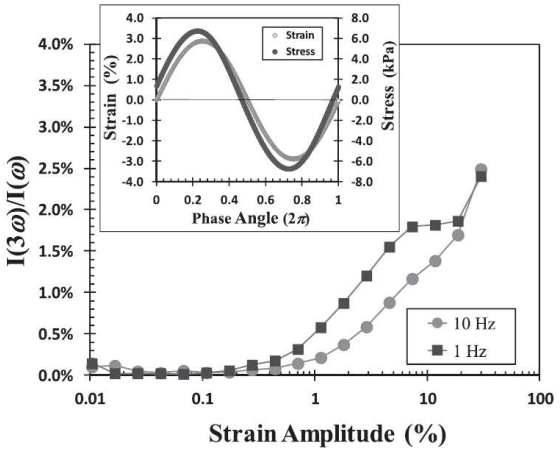

Figure 1.10. Dependence of the ratio of first and third harmonics on strain amplitude. The test material: SBR-CB rubber.

Lissajous plots offer another method to visualize rheological responses, wherein oscillatory shear deformation at a fixed amplitude is plotted against the periodic shear stress response. In the linear viscoelastic regime, these plots show an elliptical shape. By replotting the sinusoidal data of Figure 1.9 into a Lissajous plot, become visually apparent that the deviations from the elliptical shape at high amplitudes are a limited entity [30]. This observation implies that, unlike other materials exhibiting complex nonlinear responses, the classical viscoelastic quantities G' and G'' remain effective for analyzing the Payne effect in vulcanized rubber compounds.

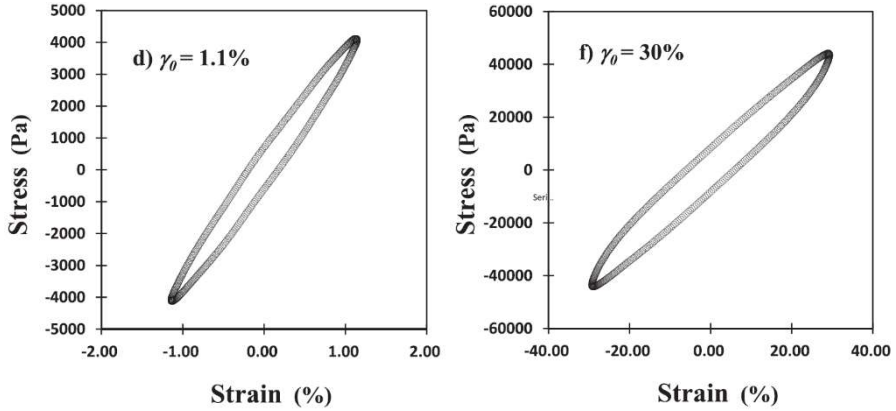

Figure 1.11. Lissajous presentation of the response of rubber to forced oscillatory shear. The test condition for cases (d)-(f): Strain-controlled mode at 10 Hz and 25 °C. The test material: SBR-CB rubber [30]

1.4.3. Reversibility and recovery aspects

Filled and unfilled rubber-like materials exhibit a stress-softening phenomenon known as the Mullins effect, which, unlike other similar effects, is irreversible at room temperature. This phenomenon has been extensively documented in various studies [51] [52] [5] [53]. When examining the Payne effect, which describes the reversible softening in elastomers, researchers have noted an additional softening effect. This is particularly evident in virgin specimens subjected to tests in which strain amplitude is first gradually increased to a maximum value and then decreased to the initial value, and the cycle is repeated more than once [54] [55] [51]. Data (Figure 1.12), particularly dynamic modulus measurements from the initial upward amplitude sweep (labeled as "up 1"), differ markedly from subsequent sweeps. This reduction in modulus is attributed to the Mullins effect and has been considered irreversible [51] [36].

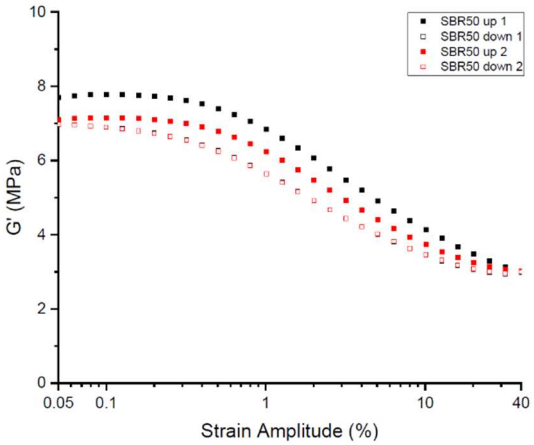

Figure 1.12. G' function of strain amplitude in increasing and decreasing amplitude sweeps driven in series tests for (a) SBR50, (b) SBR25 and (c) SBR0 [36]

To mitigate the influence of the Mullins effect, experimental procedures often involve preconditioning filled rubber samples using large strain amplitudes. This preconditioning is essential to exclude the influence of the Mullins effect from the observations, focusing solely on the reversible softening characteristics [29] [51].

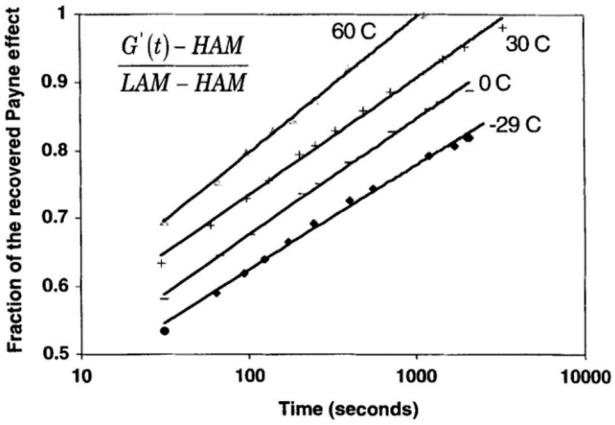

Figure 1.13. Dynamic storage modulus recovery in time at different temperatures (HAM high amplitude modulus, LAM low amplitude modulus) [29]

In literature, the term "reversibility" is frequently associated with the Payne effect in preconditioned samples. Sternstein et al. (2000) demonstrated that the low amplitude shear modulus in such samples could be restored over time, indicating a degree of reversibility and recovery [29] [56] [57] [51].

In contrast to these methods, the current study does not utilize preconditioning. This approach allows for an examination of both the reversibility and the recovery kinetics of the initial softening effect, as observed in virgin specimens. This method provides a more comprehensive understanding of the intrinsic material behavior, encompassing the reversible and the presumed irreversible softening effects.

1.4.4. Frequency-insensitive feature of Payne effect

In the study of filled rubbers, a recurring observation in the literature is that for filled rubbers the effect of measurement frequency on the dynamic storage modulus vs. shear strain amplitude gives constant shifts along the vertical direction with the increase of frequency [29] [30]. This manifests as almost parallel strain sweep curves at various frequencies, a feature clearly illustrated in following figures:

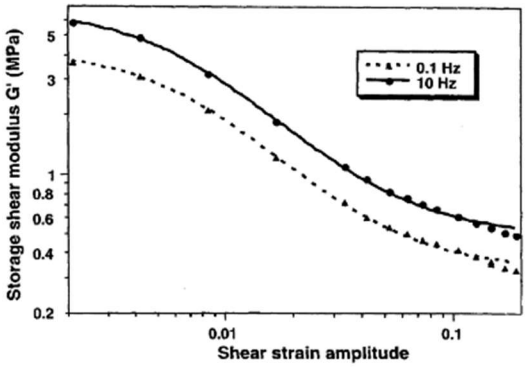

Figure 1.14. Frequency dependence of the storage shear modulus vs. dynamic strain amplitude relationship for a silica filled-silicone elastomer at 25 °C [40]

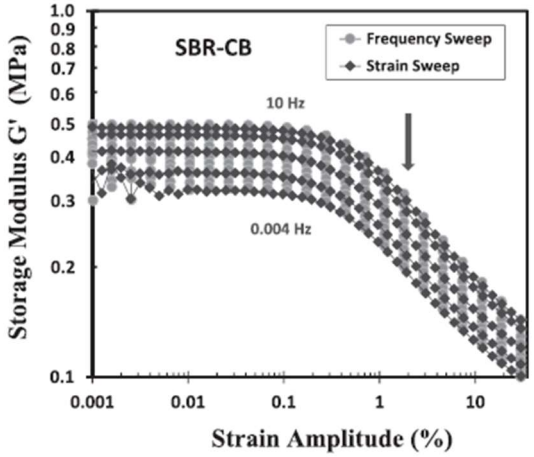

Figure 1.15. G' and G'' at 25° versus γ_0 for the SBR-CB rubber at various frequencies. The strain sweeps are performed at several fixed frequencies, 0.004, 0.04, 0.4, 4, and 10 Hz. Arrow marks the location of the G^* maximum [30]

This distinct phenomenon is referred to as the "frequency-insensitivity feature of the Payne effect" [58] [59] [60] [61]. Notably, this pattern holds true for both the storage (G') and loss (G'') components of the dynamic modulus, leading to what is termed the frequency-deformation separability principle. In essence, within both linear and nonlinear regimes, the dynamic moduli can be effectively decomposed into two components: one that depends on strain and another on frequency (1.8).

$$G'(\gamma_0, \omega) = f(\gamma_0)G'_0(\omega)$$
$$G''(\gamma_0, \omega) = g(\gamma_0)G''_0(\omega) \quad 1.8$$

Where, following the conventions of the literature, the low amplitude moduli for storage and loss are designated as G'_0 and G''_0, respectively (in this experimental work these notations are applied). This separability implies that experimental data across different frequencies can converge into a single, unified master curve. Achieving this involves normalizing G' by G'_0 and similarly G'' by G''_0 (1.9), where both G'_0 and G''_0

represent the moduli at sufficiently low strain amplitudes that exhibit linear characteristics [30].

$$\begin{cases} \dfrac{G'(\gamma_0,\omega)}{G'_0(\omega)} = f(\gamma_0) \\ \dfrac{G''(\gamma_0,\omega)}{G''_0(\omega)} = g(\gamma_0) \end{cases} \quad 1.9$$

The Figure 1.16 below illustrates this principle, showing that only vertical adjustments, influenced by frequency, are required for data alignment.

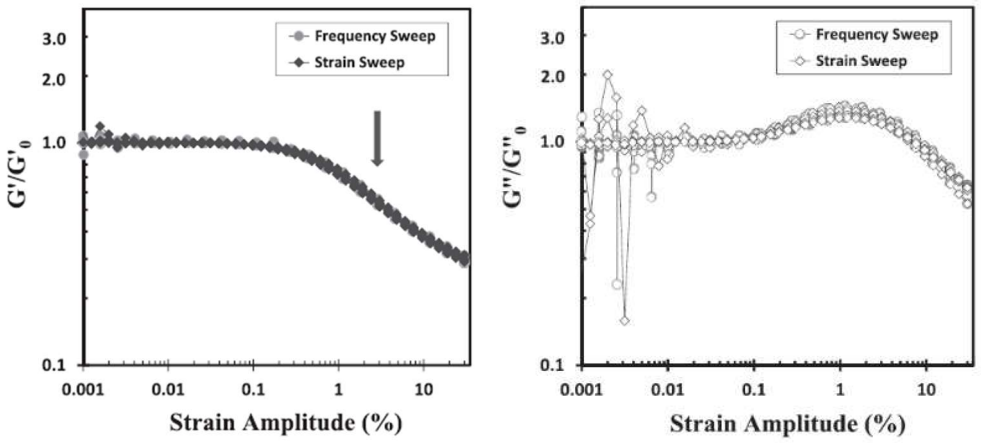

Figure 1.16. Normalized G' and G'' at 25°C versus γ_0 for the SBR-CB rubber [45]

Relying on this fundamental understanding, the current research effort to explore the extent to which the frequency-insensitivity feature of the Payne effect is observable and consistent in the present system.

2 Materials and methods

2.1. Materials and preparation

The experimental work involved testing materials comprising E-SBR 1500 (styrene-butadiene rubber), produced by Versalis S.p.A., and NBR (acryl nitrile butadiene rubber), each reinforced with silica in varying concentrations. E-SBR 1500, a standard grade of SBR used in car tires and inner tubes, is manufactured through cold emulsion copolymerization employing rosin and fatty acid soaps, containing 23% chemically bonded styrene. Versalis S.p.A. of Milan, Italy, provided the uncured E-SBR compounds in four batches differentiated by silica filler content, measured in phr (parts per hundred rubber). This metric indicates the grams of a particular component per 100 grams of rubber matrix. The four batches contain 0, 25, 50, and 75 phr of silica Zeosil 1165 MP supplied by Solvay.

It is crucial to clarify the nomenclature for all the material types, as these will be consistently used as labels throughout the detailed results report. Table 2.1 outlines these terms.

Table 2.1: Labels used in the present work to lighten the notation of the materials

Silica content [phr]	**Material notations**
0	SBR 0
25	SBR 25
50	SBR 50
60	NBR 60
75	SBR 75

In addition to the silica filler, the compounds detailed in Table 2.2 incorporated several essential ingredients, each serving a unique purpose in the rubber compounding process. The antioxidant 6PPD, or N-(1,3-dimethylbutyl)-N'-phenyl-p-

phenylenediamine, was included to protect the rubber from oxidative degradation. CBS, known chemically as N-cyclohexyl-2-benzothiazole sulfenamide, functioned as an accelerator to advance the vulcanization process. The coupling agent, Si69, or bis3-triethoxysilylpropyltetrasulfide, was crucial for enhancing the bond between the silica filler and the rubber matrix, thus improving the mechanical properties of the compounds. Lastly, zinc oxide (ZnO) served as an activator, facilitating the overall vulcanization reaction, and ensuring a uniform cure throughout the compound.

Before testing, these compounds underwent vulcanization using a compression molding press. The process involved applying 10 MPa pressure at 170 °C for 10 minutes, replicating the conditions suggested by Pirelli & C. S.p.A. and used by Luca Di Giosia with similar materials. The molds produced rubber sheets of 127x127x3 mm^3, later die-cut into rectangular specimens with dimensions 34x9x3 mm^3, as determined by Luca Di Giosia [36].

Additionally, this study analyzes NBR, reinforced with 60 phr of silica. However, due to a confidentiality agreement, details regarding NBR's supplier and composition were not available. While the silica-filled NBR sheets were thinner than the E-SBR ones, they were cut into identical rectangular shapes.

Table 2.2: Batches composition per 100 grams of E-SBR

Species [phr]	**SBR 0**	**SBR 25**	**SBR 50**	**SBR 75**
KER 1500	100	100	100	100
Silica	0	25	50	75
Si69		2	4	6
6PPD	2	2	2	2
Steric acid	2	2	2	2
ZNO	2	2	2	2
CBS	3	3	3	3
S	1	1	1	1

2.2. Dynamic mechanical tests

In this particular section, we provide a comprehensive and detailed description of the measuring instrument and the various test protocols that have been utilized in our procedures.

2.2.1. Testing apparatus

This investigation employed the Anton Paar MCR502 Rheometer, showcased in Figure 2.1 (a). Specimen testing was conducted under shear deformation in an oscillatory mode, using the torsional setup illustrated in Figure 2.1 (b). This setup features two main elements: an upper tool and a lower tool, each equipped with adjustable clamps to firmly secure the specimen. However, the clamps lack a mechanism for controlling the force applied, marking a limitation of this methodology.

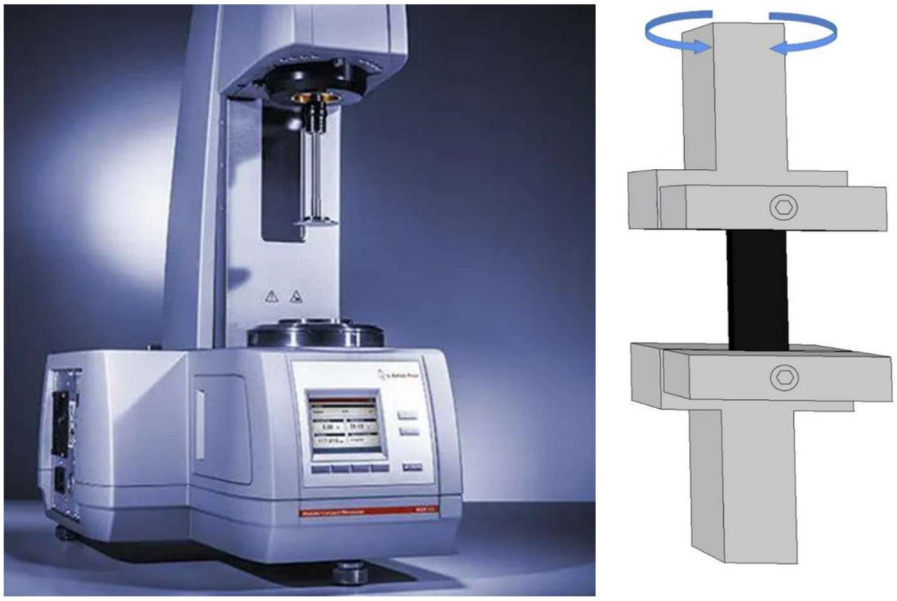

(a) (b)

Figure 2.1. Imagine of the Anton Paar MCR502 on the left (a), scheme of the torsional setup on the right (b)

Operational dynamics of the setup involve the upper clamp, which is connected to the motor via a shaft. This connection enables the induction of oscillatory shear through rotational motion. Additionally, the system permits the control of the axial force exerted on the specimen through vertical adjustments of the motor along the crosshead. The lower clamp remains static, integrated into the instrument's structure.

By inputting the precise dimensions of the rectangular specimen into the Anton Paar Rheometer, the instrument calculates the specific shear strains selected by utilizing the relationship between the deflection angle (θ) and the shear strain (γ) for rectangular

cross-sections, as outlined in Equation 2.2. By measuring the torque response of the material, the rheometer can estimate the shear modulus using Equation 2.1. This equation is derived from the approximation of Saint-Venant's exact solution for the primary torsion of rectangular specimens. Specifically, the approximation arises from omitting higher terms in the series expansion that describes the polar moment of inertia J [36]. Nevertheless, this equation is commonly used in most commercial rheometers.

$$G = \frac{M}{DJ} = \frac{3ML}{\theta w t^3 g_{sv}(n)} \tag{2.1}$$

with

$$\theta = \frac{\gamma LC}{t} \tag{2.2}$$

$$C = \frac{1}{[1 - 0.378n^{-2}]} \tag{2.3}$$

$$g_{sv}(n) \cong 1 - \frac{192}{n\pi^5}\left(tanh\left(n\frac{\pi}{2}\right) + 0.004524\right) \tag{2.4}$$

$$n = \frac{w}{t} \tag{2.5}$$

$$D = \frac{\theta}{L} \tag{2.6}$$

Owing to the inability to precisely control the clamping force, a preliminary analysis was conducted to quantify the associated variability. The findings and detailed discussions of this aspect are presented in the respective subchapter, providing a deeper understanding of its impact on the overall experimental results (Section 2.4).

It is essential to briefly summarize a few observations regarding the testing apparatus that emerged during the analysis:

- The instrument with this setup and specimen geometry has some difficulties at high amplitudes (30%) especially at high frequencies (20 rad/s), maybe due to some slippage phenomena
- The periodic cleaning of the clamps reduces the just mentioned risk
- The lack of a dynamometric torque wrench leads to an increase of the system variability

2.2.2. Sinusoidal oscillatory test in simple conditions

To characterize the viscoelastic behavior of the samples, various histories of oscillatory sinusoidal deformations under shear conditions were imposed. These different deformation profiles aimed to unravel the complex nonlinearity inherent in the reinforced elastomer being studied. Typically, in line with the instrument manufacturer's recommendations, a 1 N tension normal to the sample's cross-section augments the sinusoidal oscillations.

The chosen approach, with its focus on the amplitude of dynamic strain, the time, and the frequency of application, is essential for an in-depth analysis of the material's viscoelastic properties. The experimental parameters considered are outlined in Equation 1.1 where γ_0 is the amplitude of the shear strain and ω is the frequency.

$$\gamma(t) = \gamma_0 \sin(\omega t) \qquad 2.7$$

2.2.3. Shear Strain amplitude sweep tests

The most utilized test for investigating the Payne effect involves deforming the specimen with progressively increasing strain amplitudes, γ_0. This method typically focuses on the material's steady-state behavior, therefore the acquisition of the data at each step waits until the steady state is reached. The specific parameters utilized in these tests of the present work are reported in the table that follows:

Table 2.3: Control parameters of the increasing strain amplitude test

γ_0 [%]	γ_0 [%]	Frequency [rad/s]
0,01	30	5

The scheme of this standard test method is depicted in Figure 2.2.

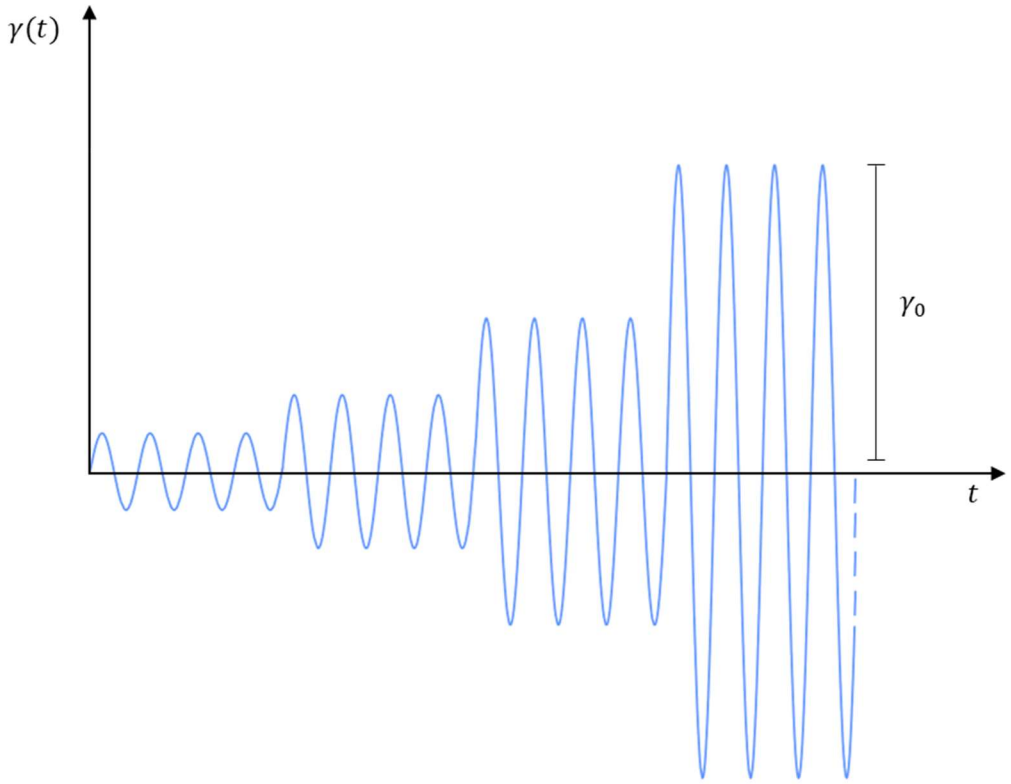

Figure 2.2. Scheme of an oscillatory applied strain test with a logarithmical increasing strain amplitude γ_0

2.2.4. Series of shear strain amplitude sweep

In addition to this, an extra test protocol has been selected to examine the reversibility of the Payne effect and the impact of stretching on the material's characteristics. This additional method involves conducting a series of amplitude sweep tests in succession, and the testing protocol is detailed in Table 2.4 below. The nomenclature was set in such a way that the initial amplitude sweep is termed "sweep #0", emphasizing the pristine condition of the sample without any prior strain application. By this logic, the subsequent amplitude sweep is labeled "sweep #1," indicating the material has previously been subjected to one amplitude sweep, and so on.

Table 2.4: Successive strain amplitude sweep test protocol, including its parameter nomenclature; the rest time $\tilde{t}$ is set to a different value depending on the material and test frequency.

Interval	Initial γ_0 [%]	Final γ_0 [%]	ω [rad/s]	Rest time	Nomenclature
1	0,01	30	$\tilde{\omega}$		Sweep #0
2				$\tilde{t}$	
3	0,01	30	$\tilde{\omega}$		Sweep #1
4				$\tilde{t}$	
5	0,01	30	$\tilde{\omega}$		Sweep #2

Between these sweep tests, a rest period is included. Each material underwent the documented procedure for different frequencies which are chosen among these values: 0,1, 1, 5, 10, and 20 rad/s.

The schematic view of this series of amplitude sweeps is illustrated in Figure 2.3.

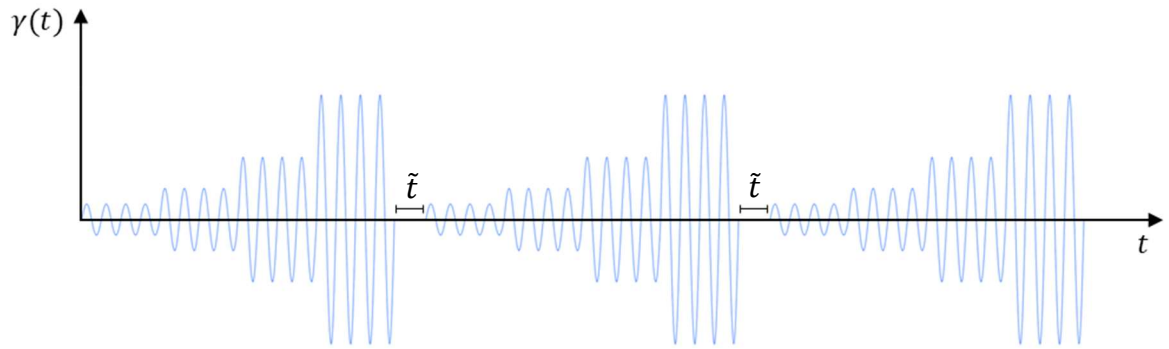

Figure 2.3. Scheme of increasing and decreasing amplitudes sweeps driven in series test

A possible variant of the previous protocol is detailed in Table 2.5, where the rest time is no more fixed but is different between sweeps #0 and #1 respect to the rest time between the sweeps #1 and #2. The rest times are variables but in general $\hat{t}_1$ is minor than $\hat{t}_2$.

Table 2.5: this table outlining two amplitude sweeps intervals, each detailed with its corresponding parameters and divided by a variable long rest time $\hat{t}$

Interval	**Initial γ_0 [%]**	**Final γ_0 [%]**	**ω [rad/s]**	**Rest time**	**Nomenclature**
1	0,01	30	20		Sweep #0
2				$\hat{t}_1$	
3	0,01	30	20		Sweep #1
4				$\hat{t}_2$	
5	0,01	30	20		Sweep #2

The protocol previously detailed was used to assess the response at various times. However, due to time restrictions in the experimental phase of the thesis, this test was exclusively performed on SBR 50 and 75, and only at a frequency of 20 rad/s.

2.2.5. Series of strain amplitude sweeps followed by a constant low strain amplitude test

It has been demonstrated that following a test after increasing deformation amplitudes, the dynamic moduli exhibit a significant time dependency (1.4.3). The study's approach to evaluating the system's recovery capabilities—in terms of both the kinetics and the extent of recovery of the linear modulus of unstrained material—involved a specific test. This implied imposing a constant low strain amplitude test subsequent to the series of amplitude sweeps already described. The experimental details of the test protocol can be found in Table 2.6, which includes only the last of the amplitude sweep tests, referred to as "sweep #2". The protocol was applied considering the frequencies of 5, 10, and 20 rad/s.

Table 2.6: table outlining a series of test intervals, each detailed with its corresponding parameters.

Interval	Initial γ_0 [%]	Final γ_0 [%]	ω [rad/s]	Rest time	Nomenclature
1	0,01	30	$\tilde{\omega}$		Sweep #2
2				6 s	
3	0,01		$\tilde{\omega}$		Recovery

Following the amplitude sweep series and a six-second rest interval, a fixed low strain amplitude at a constant frequency is then employed to track the recovery over time of the low amplitude storage modulus, recorded as $G'_{0\#3}(t)$, and compared to the initial virgin modulus $G'_{0\#3}$ (#0). The interlude of six seconds is mandated by the equipment's limitations when shifting from a high amplitude (30%) to a low amplitude (0.01%), particularly due to system inertia at elevated frequencies.

The protocol was applied to all material types previously examined. The analysis will particularly concentrate on how the low amplitude moduli progress over time and whether the original pristine modulus ($G'_{0\#0}$) is fully regained. Thereafter, the chapter will delve into the temporal changes of the Payne effect curve beyond the initial low amplitude response.

To schematically explain the protocol detailed in Table 2.6, the test sequence is illustrated in Figure 2.4.

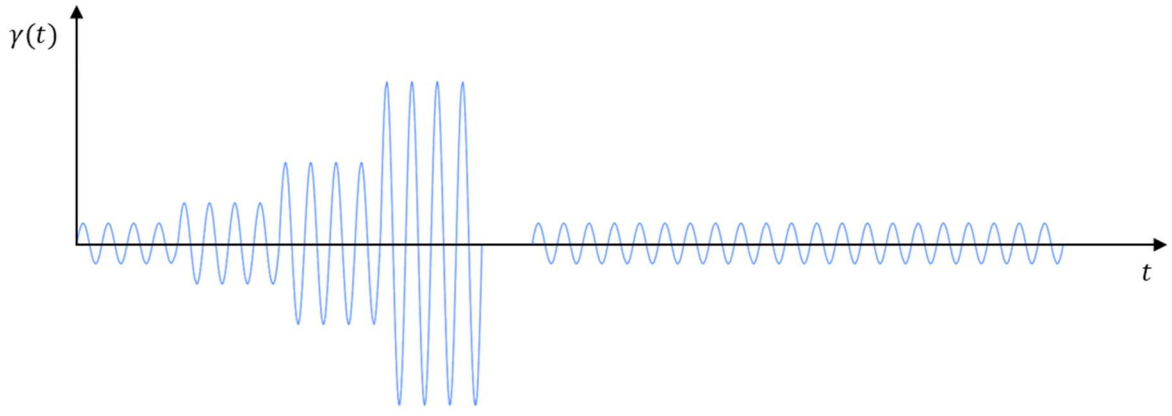

Figure 2.4. Scheme of a sequence of strain amplitude sweep test followed by a constant amplitude of strain test

2.2.6. Frequency sweep test

The final type of test adopted involves applying a logarithmically increasing frequency, at a constant strain amplitude. This test was conducted to examine how the moduli are affected by frequency in the low amplitude linear range. It has to be said that samples tested using this method are virgin materials.

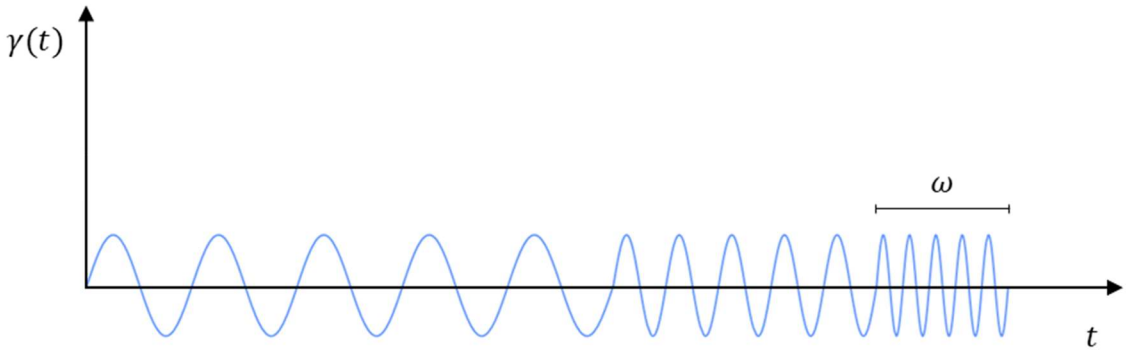

Figure 2.5. schematic view of the oscillatory applied strain with a logarithmical increasing frequency ω in time

2.3. Sample geometry

The determination of a sample geometry ensures accurate measurements with the Anton Paar MCR502 rheometer, was informed by extensive preliminary work [36]. Styrene-Butadiene Rubber (SBR) bars with length 34mm and width 9mm were die cut from 3mm thick slabs. The dimensions followed both theoretical considerations and empirical findings.

In the primary torsion problem of rectangular bars as described by De Saint-Vénant [36], sections perpendicular to the rotational axis of the specimen bar are assumed to be free to warp. Therefore, out-of-plane displacements along the rotational axis occur. Actually, when the sample is twisted in torsion, axial stresses occur near the clamps as the warpage is hindered. Then secondary torsion arises from tangential stresses that balance those normal stresses induced by prevented warping deformations. Such an effect can be seen as a localized phenomenon close to the constraining areas, and its effect on the overall modulus measurement depends on the specimen length-to-width ratio and its cross-section geometry (or thickness to width ratio) [34].

Since the instrument takes only into account the primary torsion component a significant higher shear modulus may be measured; for this reason, the geometry analysis aims to minimize artefacts choosing the values of the cross-section aspect ratio and the length-to-width ratio that would minimize the overestimation of the modulus.

In general, a square cross-section (that is a width-to-thickness ratio equal to 1) and a length-to width ratio higher than 3 are recommended [62].

At the other hand there're some constraints which have to be taken into account:

- The torque range of the instrument (from 0.002 μNm to 200 mNm)
- Maximum thickness allowed by the setup (4 mm)
- The equations used by the instrument have a maximum limit of validity in terms of deflection angle ($\theta < 180°$).

Starting with the assumption that the shear modulus G of SBR grades is around 1 MPa, L. Di Giosia in 2022 [36] chose a cross-section aspect ratio of 3 with a thickness of 3 mm. These dimensions were selected based on the maximum thickness, the smallest measurable torque, and the most suitable cross-section aspect ratio.

Additionally, taking into account the constraint on the deflection angle and the requirement for a length-to-width ratio greater than 3, a length of 20 mm was determined. Also, considering the necessity to secure the sample with a clamping length of 14 mm, the overall length of the sample was established to be 34 mm.

The decision to apply these results in this study is further justified by the fact that the materials being investigated here are similar to those analyzed in [36].

In the case of the NBR material used in this research, the discussion around sample geometry was not necessary, as the NBR samples came pre-sized at 34 mm in height, 9 mm in width, and 2 mm in thickness. This pre-determined dimension meant that our focus could remain on other experimental variables, with the geometry already set.

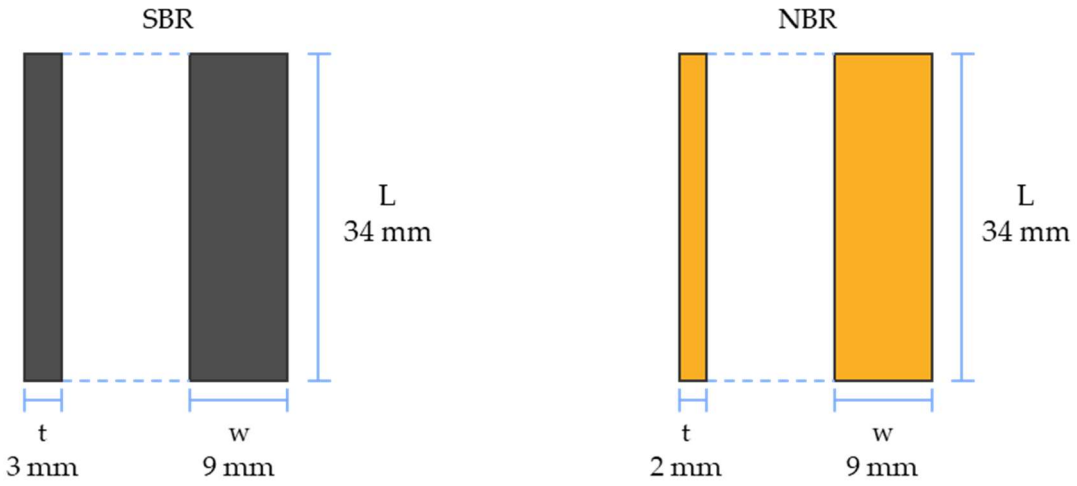

Figure 2.6. Scheme of the standard specimen dimensions representing SBR and NBR with their dimensions

2.4. Sample installation errors analysis

At the outset of this chapter, we examine the errors inherent in the sample installation process, noting how they can compromise measurement accuracy. it is imperative to address the variability introduced during the clamping operation, which currently lacks a tool to regulate the clamping force. Additionally, the geometric placement of the sample relies solely on visual estimation, which inherently introduces a degree of inaccuracy into the measurements. Furthermore, it's important to point out that this variability is influenced by the methodology and the operator involved.

Compounding these issues is the viscoelastic nature of the material in question. The stress state induced by the clamps evolves over time following deformation, which could further affect the integrity of the measurements. Given these complexities, it is crucial to ascertain the most effective testing methodologies that minimize potential errors. In fact, to minimize potential errors coming from this aspect for all the analysis presented in this experimental work, it's been predetermined a resting period post-clamping of 120 s to wait before the specific test would start.

The subsequent sections will delve into the analytical exploration of the before mentioned issues, with a focus on both the control of clamping forces and the precision of geometric positioning. It is essential to note that the analyses to follow have been conducted on virgin samples, ensuring that the findings reflect the initial state of the material devoid of any pre-existing stress or deformation influences.

2.4.1. Clamping and positioning error

To isolate the variability introduced during the clamping and positioning phase, modulus measurements for SBR compounds with variable silica contents are recorded at a fixed strain amplitude (0,01%) and frequency (20 rad/s). The protocol devised is described in Table 2.7: Protocol for the investigation of the positioning and clamping error. , and was applied 5 consecutive times on each sample considered in this investigation.

Table 2.7: Protocol for the investigation of the positioning and clamping error.

Steps	Description
1	Positioning and clamping
2	Rest time (120 s)
3	Oscillatory measurement (γ_0 = 0,01 %; ω = 20 rad/s)
4	Removal
5	Rest time (10 min)

The removal of the sample is followed by a ten-minute relaxation period, after which the step sequence is reiterated on the same sample, so as to minimize confounding variables such as minor inconsistencies in material composition or sample geometry.

The results (Figure 2.7) display the dependence of G′ and G′′ on silica content (in parts per hundred rubbers - phr), with the error bar related to specimen positioning and clamping.

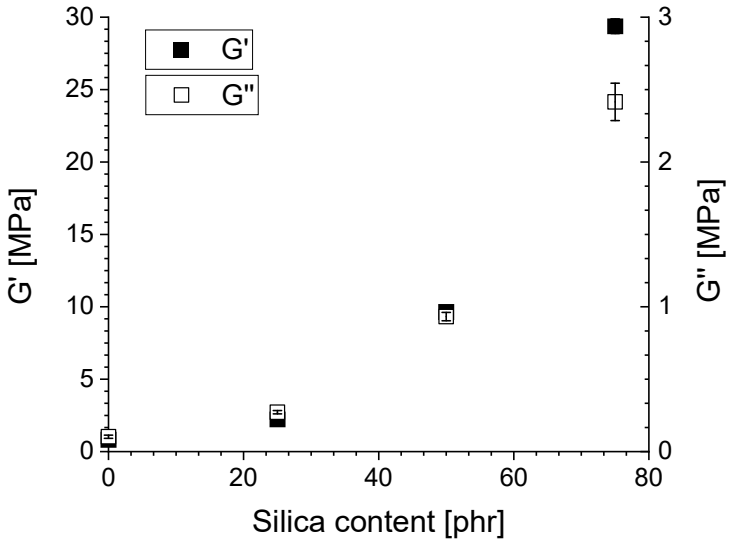

Figure 2.7. Storage (G') and loss (G'') modulus in tests performed at γ_0 = 0,01 %; ω = 20 rad/s for each silica content (0, 25, 50, 75 phr) in SBR

The provided graph presents the mean values of the storage and loss moduli obtained from five trials, with error bars representing the maximum dispersion (difference between the highest and the lowest values) of the data points. Notably, the variability becomes more pronounced in SBR samples containing higher levels of silica, particularly in terms of the loss moduli. To clearly discern the impact of these variabilities on the measurements, a comparison of the relative maximum dispersion (relative error) across different mixtures is presented. Therefore, each data point and corresponding error bar have been normalized to the average modulus value for each mixture, as depicted in the figure.

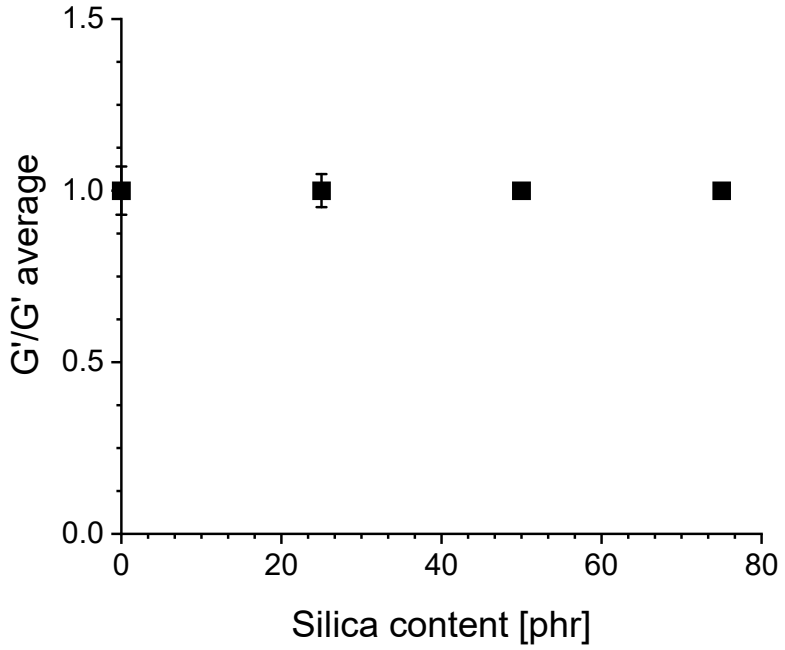

Figure 2.8. Normalized storage modulus with error bars showing the relative maximum dispersion of the data as a function of the silica content in SBR

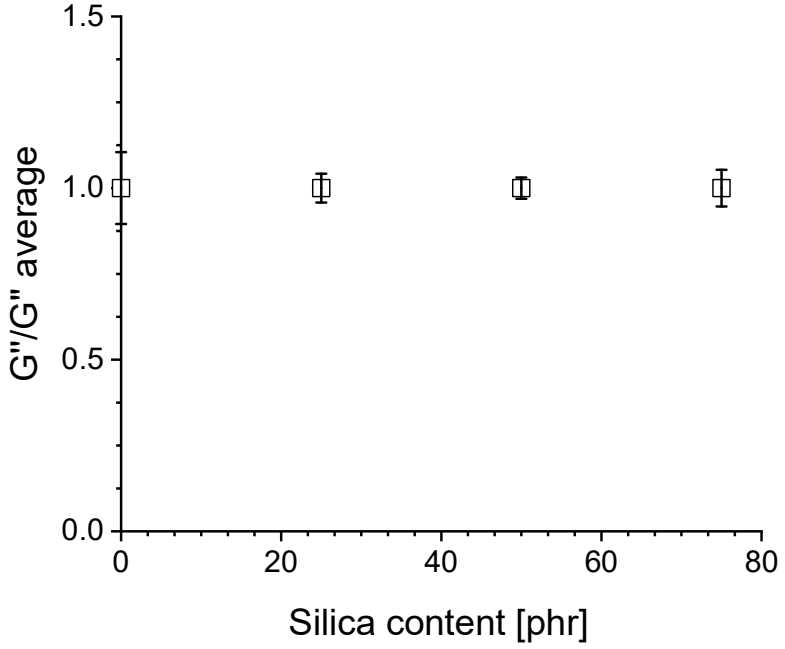

Figure 2.9. Normalized loss modulus with error bars showing the relative maximum dispersion of the data as a function of the silica content in SBR

The analysis reveals a more significant relative effect of the positioning and clamping procedures on samples with lower silica content in both components of modulus, with maximum errors of around 10% relative to the average measured moduli. In general,

for silica-filled SBR and neat SBR, the errors remain below 10% for storage moduli and are about 10% or less for loss moduli.The effect of filler content is significantly higher, so it can be concluded that although clamping and positioning operations do impact the measurements, their influence is not so significant.

This preliminary examination has been undertaken to quantify potential errors that may influence the outcomes, particularly in studies requiring the sample to be removed post-measurement and subsequently reinstalled and tested after a certain duration.

3 Experimental results

In this chapter attention is directed towards the nonlinear response exhibited by filled rubbers when subjected to increasing strain amplitude, known as the Payne effect. Specifically, the results are intended to demonstrate how various factors like filler content, material history, time, and frequency influence this nonlinear phenomenon.

3.1. Payne effect

3.1.1. Filler effect on storage and loss moduli

Dynamic mechanical analysis, particularly through increasing strain amplitude tests commonly referred to as amplitude sweeps, is the prevalent method for examining the nonlinear behavior characteristic of filled rubber, including the Payne effect.

The following figures illustrate the dynamic moduli's non-linear dependence on strain amplitude on a double logarithmic scale, offering a comparative view of the different non-linear viscoelastic behaviors of various materials, as shown in Figure 3.1 and Figure 3.2. The SBR samples with 0, 25, 50, and 75 parts per hundred rubbers (phr) of silica are represented by squares shaded in varying degrees of grey, while the NBR with 60 phr of silica is denoted by triangles.

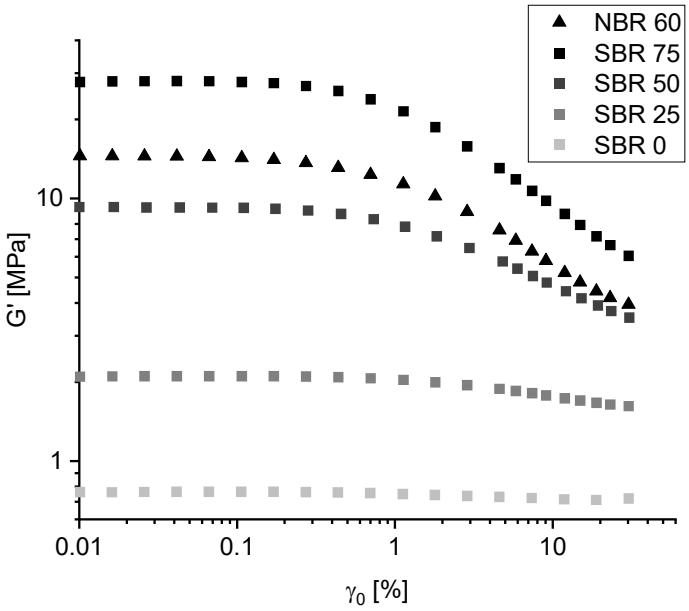

Figure 3.1. Storage modulus versus on the strain amplitude additionally showing the dependency on the filler content (SBR mixtures are represented as squares with different scales of grey, NBR 60 is represented with triangular symbols)

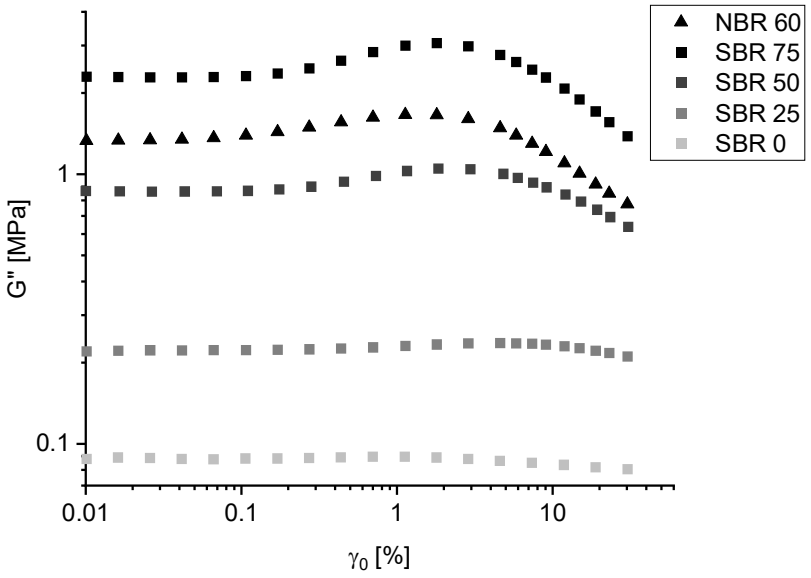

Figure 3.2. Loss modulus versus on the strain amplitude additionally showing the dependency on the filler content (SBR mixtures are represented as squares with different scales of grey, NBR 60 is represented with triangular symbols)

Figure 3.1 captures the storage modulus's behavior, where filled rubbers display the anticipated Payne effect: an initial linear response at low strain amplitudes followed

by a softening up to the maximum amplitude applied for all. As expected unfilled rubber, SBR 0, does not display this nonlinearity in the shear amplitude range investigated. The filler effect is particularly noticeable in Figure 3.3 and Figure 3.4 where the low amplitude moduli and the moduli at the highest amplitude (30%) are plotted as function of the silica content. The presence of filler substantially increases rubber stiffness—evidenced by an increase of the low amplitude moduli that is at least an order of magnitude higher for SBR 50 and 75 and NBR 60.

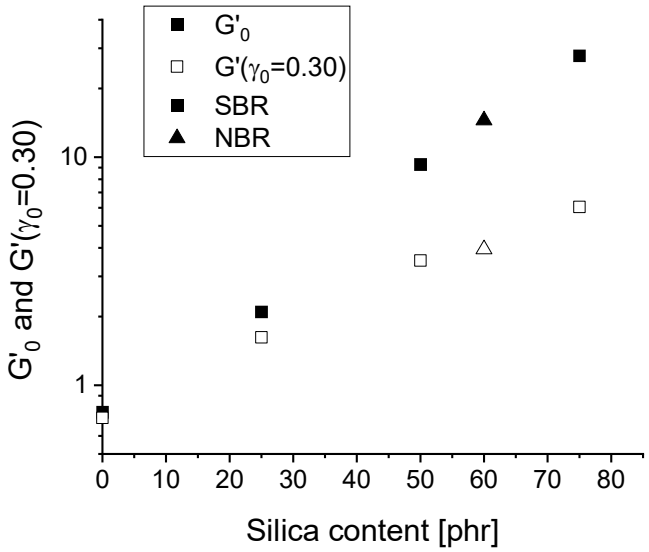

Figure 3.3. Storage moduli at low amplitudes G'_0 (full symbols) and at amplitude 30% after the Payne effect $G'(\gamma_0 = 0.30)$ (empty symbols) for SBR (squares) and NBR (triangles)

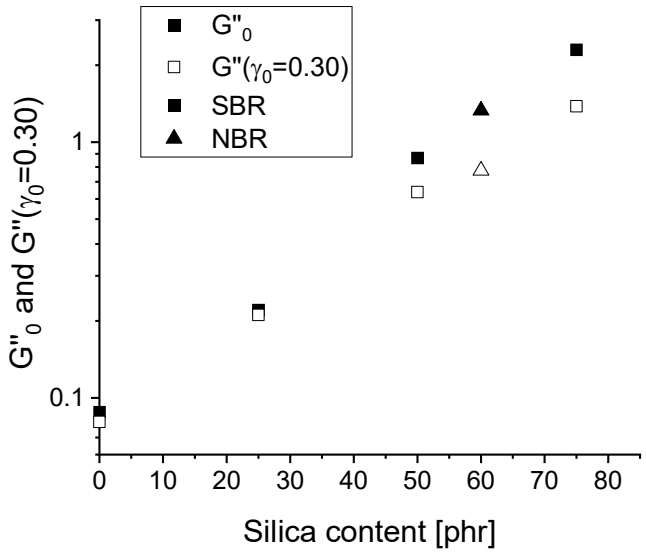

Figure 3.4. Loss moduli at low amplitudes G′$_0$ (full symbols) and at amplitude 30% after the Payne effect $G'(\gamma_0 = 0.30)$ (empty symbols) for SBR (squares) and NBR (triangles)

These graphs also reveal the damaging effect, indicated by the difference between the full and empty symbols, which intensifies with increasing silica content. This may be due to a higher proportion of chains being desorbed, as a greater concentration of particles leads to a more complex filler-rubber network.

However, the materials do not exhibit the distinct second plateau often associated with the Payne effect curve [38] at the highest amplitudes obtainable with the selected sample geometry and testing configuration.

Also the loss modulus graph versus strain amplitudes agrees with the trends reported in literature [38], characterized by a linear response at low amplitudes and a peak at medium amplitudes, which coincides with the onset of storage modulus softening. Like the storage modulus, an increase in filler content results in a heightened loss modulus curve. Additionally, this increment marginally shifts the peak of the curve towards lower amplitudes, as shown in Figure 3.2.

As already discussed in chapter 1, the mechanisms contributing to the storage modulus's softening effect are a subject of debate in the literature. One explanation could be the gradual detachment of rubber chains from the filler surfaces under increased strain, leading to the disintegration of the filler-rubber network at high amplitudes. Furthermore, the silica particles' ability to form filler-filler networks, which may also suffer damage under strain, as discussed in Section 1.2.1, could play a role. This hypothesis helps to shed light on the observation that higher silica content within the matrix correlates with stronger networks and phase interactions, ultimately enhancing the material's properties.

3.1.2. Investigation on the linearity of the oscillatory responses

Dynamic modulus analysis relies on the assumption that the material behaves linearly, meaning the response to a sinusoidal input is also sinusoidal. This is consistent with the independency of G' and G'' on shear strain amplitude. However, filled rubbers exhibit a dependence of G' and G'' on the amplitude of oscillating deformation, indicating a nonlinear behavior. Despite this nonlinearity, literature reports cases in which such materials still display a sinusoidal response, possibly due to the crosslinks created during vulcanization. Verifying this behavior is essential for validating the use of storage (G') and loss (G') moduli as meaningful representations.

One method to investigate whether the shear stress response is sinusoidal is by graphically plotting the shear stress ($\tau(t)$) measured in a cycle against the applied shear strain ($\gamma(t)$) for a given strain amplitude and frequency. This data representation is known as Lissajous plot, and for a linear viscoelastic material, it has an elliptical shape. Deviations from this shape indicate nonlinearity.

Lissajous plots presented here (Figure 3.5, Figure 3.6, Figure 3.7, Figure 3.8) reflect the material's behavior at medium and high strain amplitudes where nonlinear softening occurs. Visually, there appears to be some distortion respect to an elliptical shape.

(a)

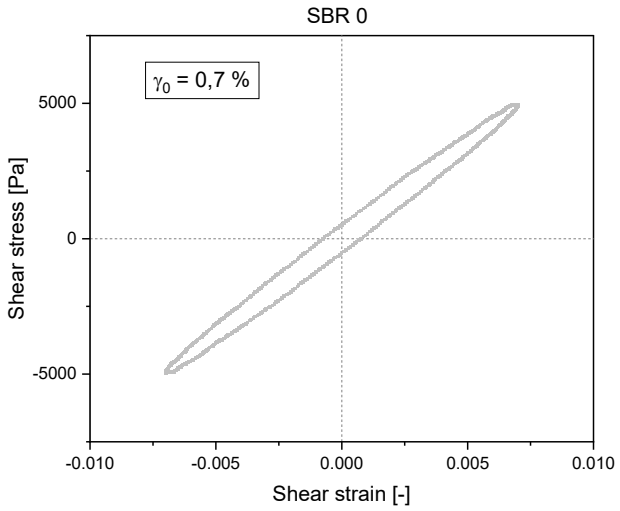

(b)

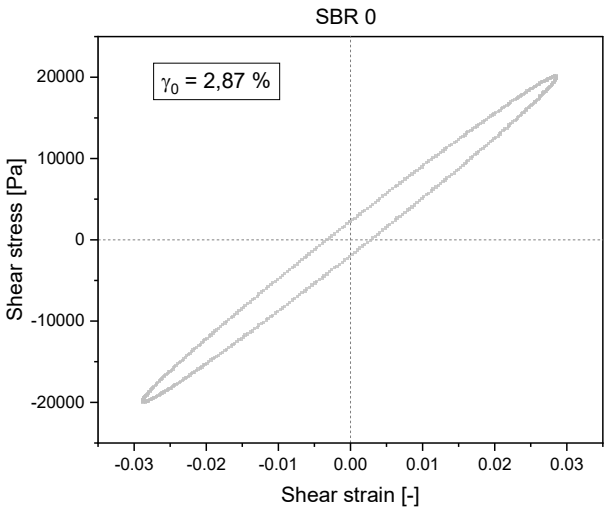

(c)

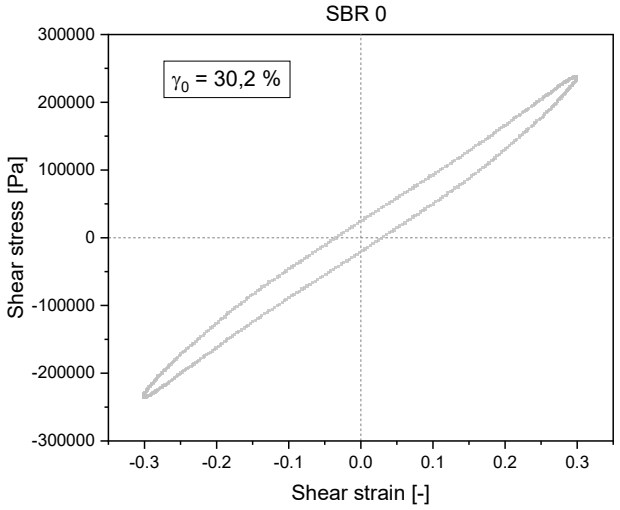

Figure 3.5. Lissajous plots for SBR 0 at strain amplitudes of 0,7% (a), 2,87% (b) and 30,2% (c), with both measured at a frequency of 10 rad/s

(a)

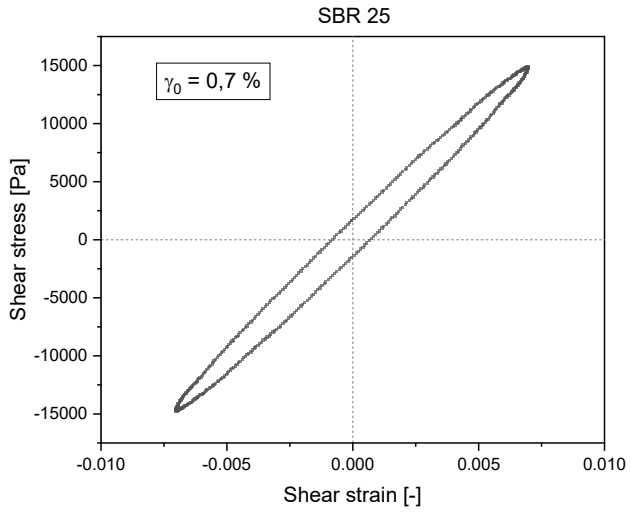

(b)

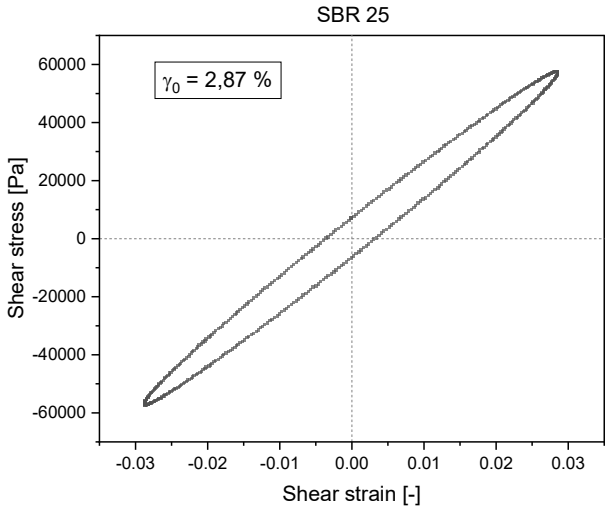

(c)

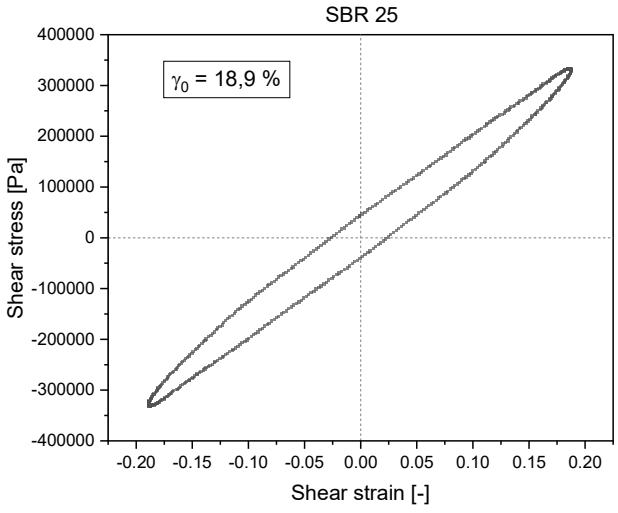

Figure 3.6. Lissajous plots for SBR 25 at strain amplitudes of 0,7% (a), 2,87% (b) and 30,2% (c), with both measured at a frequency of 10 rad/s

(a)

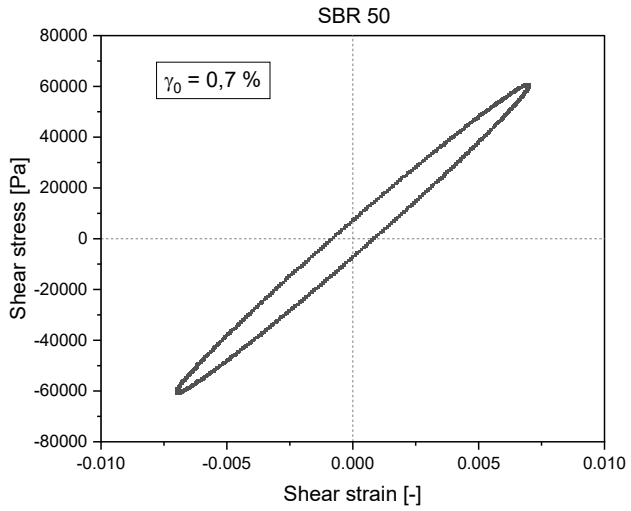

(b)

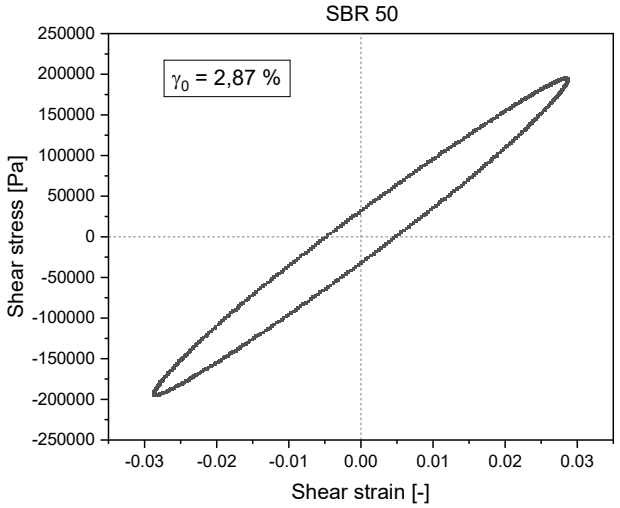

(c)

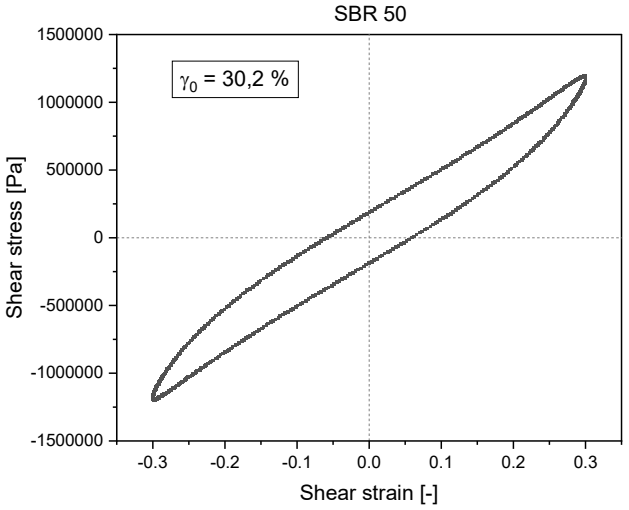

Figure 3.7. Lissajous plots for SBR 50 at strain amplitudes of 0,7% (a), 2,87% (b) and 30,2% (c), with both measured at a frequency of 10 rad/s

(a)

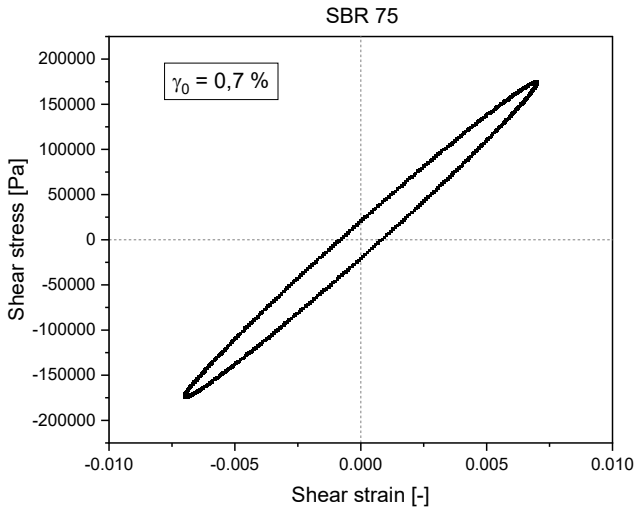

(b)

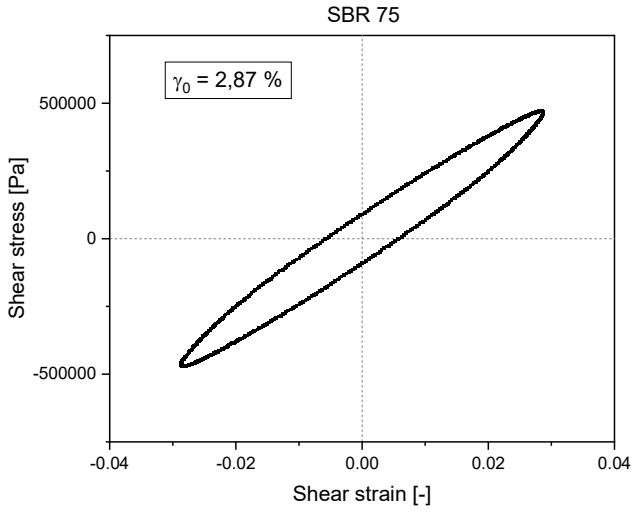

(c)

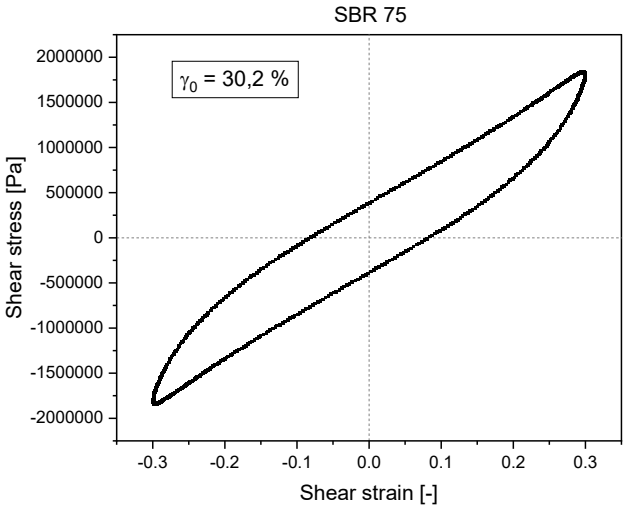

Figure 3.8. Lissajous plots for SBR 75 at strain amplitudes of 0,7% (a), 2,87% (b) and 30,2% (c), with both measured at a frequency of 10 rad/s

To quantify any deviations, Fourier Transform (FT) rheology is employed (Figure 3.9), which evaluates the nonlinearity in terms of the ratio of the intensities of higher harmonics (I(nω)) to the first harmonic (I(1ω))—the latter representing the sinusoidal linear response. Specifically, ratio of the third harmonic (I(3ω)) to the first harmonic (I(1ω)) is considered because the intensity of higher harmonics is substantially lower, often to the point of being negligible.

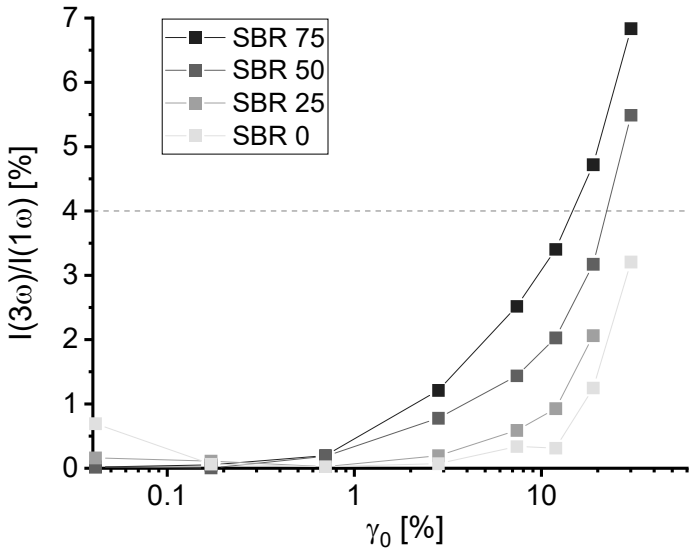

Figure 3.9. Graph depicting the ratio of the third harmonic intensity to the first, plotted against strain amplitude for different SBR mixtures, each distinguished by a shade of gray

Literature suggests that when the ratio I(3ω)/I(1ω) is less than 4%, the influence of higher harmonics can be disregarded as insignificant [30], theoretically underpinning the representations of storage and loss moduli. The graph (Figure 3.9) displays this ratio for various SBR compositions. For SBR 50 and 75, ratios at amplitudes around 20% and 30% slightly exceed the 4% threshold, but not to a degree considered significantly higher.

Consequently, subsequent experimental work presented here will overlook the presence of higher harmonics, with an understanding that data points at higher strain amplitudes may incorporate a margin of error.

3.2. Payne effect reversibility

The concept of the Payne effect's reversibility is a recurring topic within the field, typically presented alongside the close irreversible Mullins effect [36] [29]. This subchapter is dedicated to an in-depth exploration of these phenomena, emphasizing how the system's past deformation history and time have affected its behavior.

3.2.1. Series of consequent strain amplitude sweeps

The inspiration for this investigation is based on different views of several authors [36] [29]. Hence, a series of constant amplitude sweeps is implemented to initiate the investigation of the reversibility of the Payne effect. To this end, a succession of increasing amplitude sweep tests is applied to the materials considered in the thesis. In line with the observations noted in the Theory chapter 1.4.3, where the storage modulus experiences a recovery to the linear low strain amplitude moduli after the test, a fixed rest period is maintained between any successive amplitude sweeps within the series.

Following the procedure explained in the section 2.2.3, the sequence of amplitude sweeps conducted at 20 rad/s across various materials yields experimental data for $G'(\gamma_0)$ and $G''(\gamma_0)$ presented in the figures (Figure 3.10, Figure 3.11, Figure 3.12, Figure 3.13).

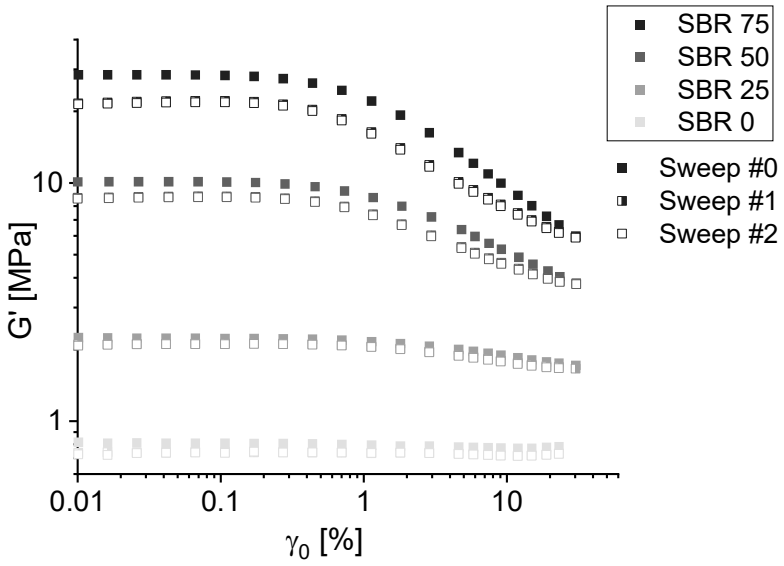

Figure 3.10. Storage modulus as function of the strain amplitude applied at 20 rad/s, materials SBR 0, 25, 50 and 75 are represented as squares with decreasing transparency for increasing filler content; the three sweeps are shown for each material: a full symbol for sweep #0, half-full symbol for sweep #1 and empty for sweep #2

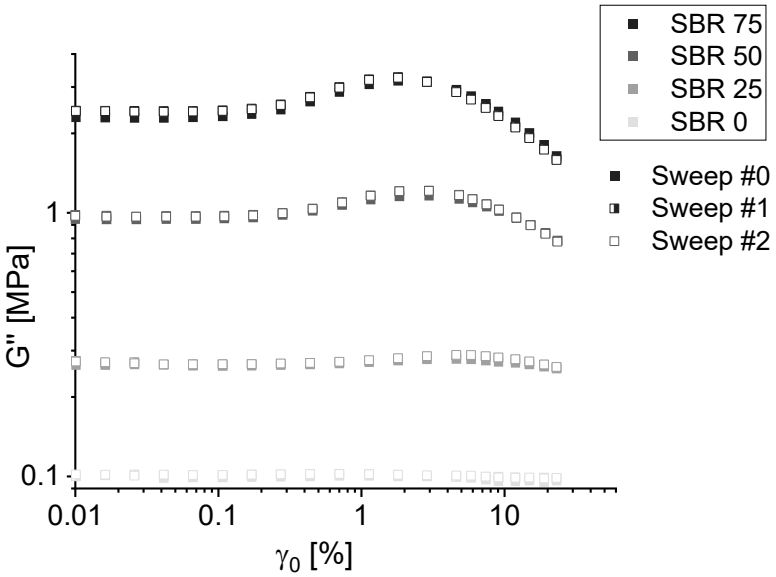

Figure 3.11. Loss modulus as function of the strain amplitude applied at 20 rad/s, materials SBR 0, 25, 50 and 75 are represented as squares with decreasing transparency for increasing filler content; the three sweeps are shown for each material: a full symbol for sweep #0, half-full symbol for sweep #1 and empty for sweep #2

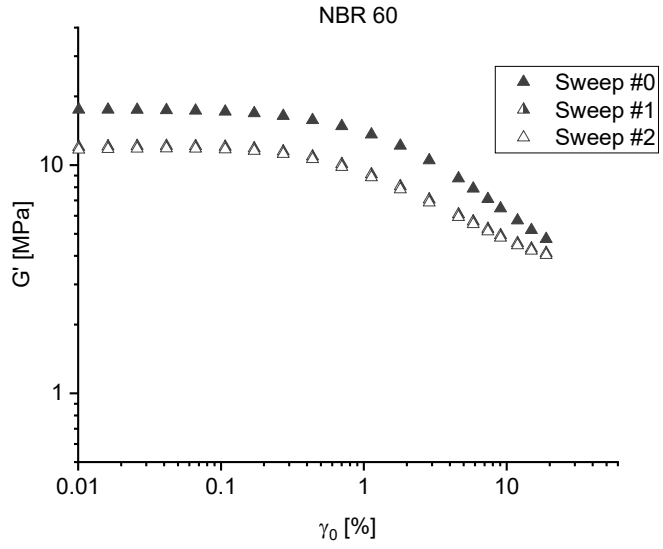

Figure 3.12. Storage modulus as function of the strain amplitude applied at 20 rad/s, material NBR 60 is represented as triangles; the three sweeps are shown as before a full symbol for sweep #0, half-full symbol for sweep #1 and empty for sweep #2

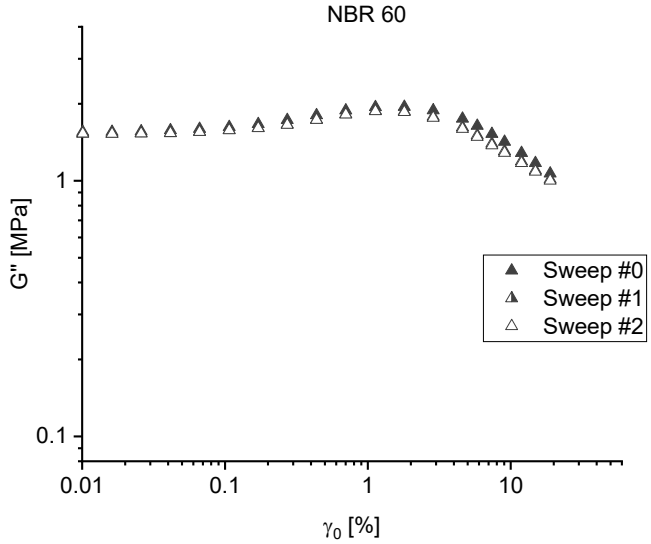

Figure 3.13. Loss modulus as function of the strain amplitude applied at 20 rad/s, material NBR 60 is represented as triangles; the three sweeps are shown as before a full symbol for sweep #0, half-full symbol for sweep #1 and empty for sweep #2

The analysis of filled SBR and NBR materials illustrates a marked contrast between the response of the initial, unstrained material in sweep #0, and in the subsequent sweeps, numbered "#1-#2". Notably, there is an evident decrease in G_0' and a limited increase in G_0'' for sweeps #1 when compared to the virgin curves (better seen in Figure 3.14, Figure 3.15, Figure 3.16, Figure 3.17). In contrast, the subsequent sweeps, after the virgin one, display overlapping curves with consistent plateau values, indicating no significant change after the first sweep.

Despite initial expectations that the unreinforced SBR would remain unaffected by softening following high strain amplitude applications, due to the absence of silica, minor variations are still noticeable across different sweeps. This observed behavior suggests that viscoelasticity may be contributing to these subtle changes.

The observed overlap of curves in sweeps #1-#2, often referred to as "reversibility" in literature, appears to be a consistent feature irrespective of the frequency employed or the various fixed rest times selected.

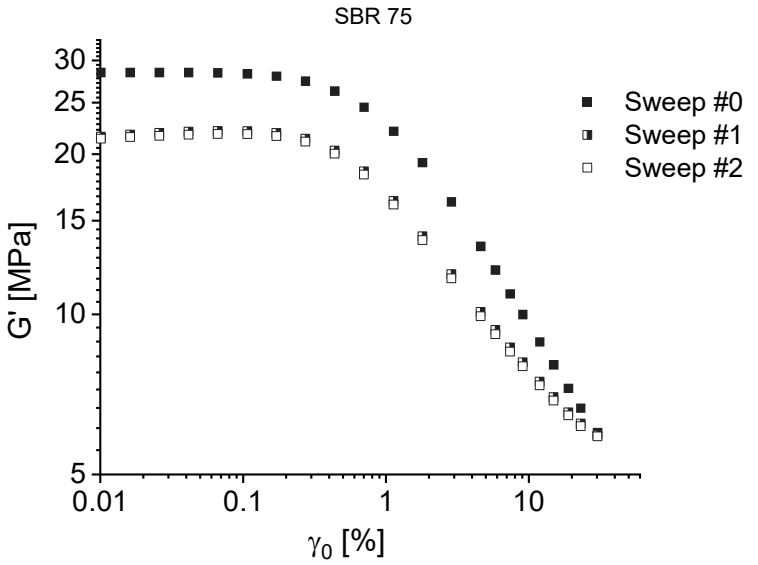

Figure 3.14. Zoom in on the storage modulus plot of SBR 75

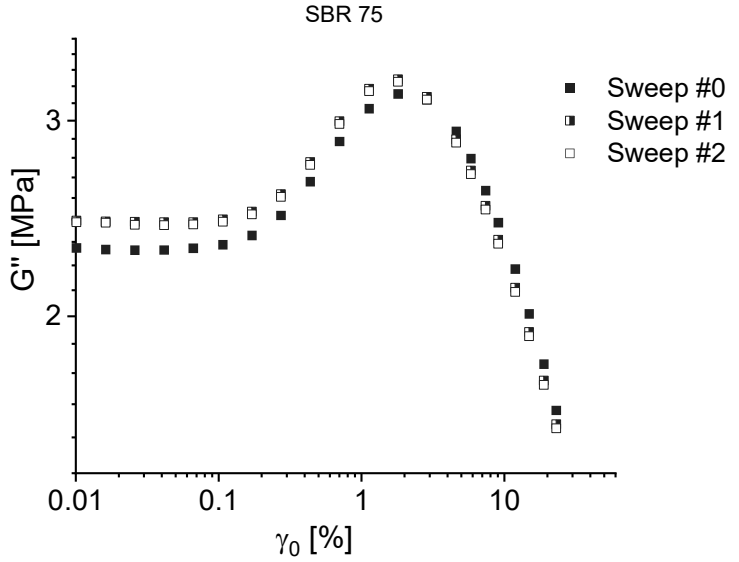

Figure 3.15. Zoom in on the loss modulus plot of SBR 75

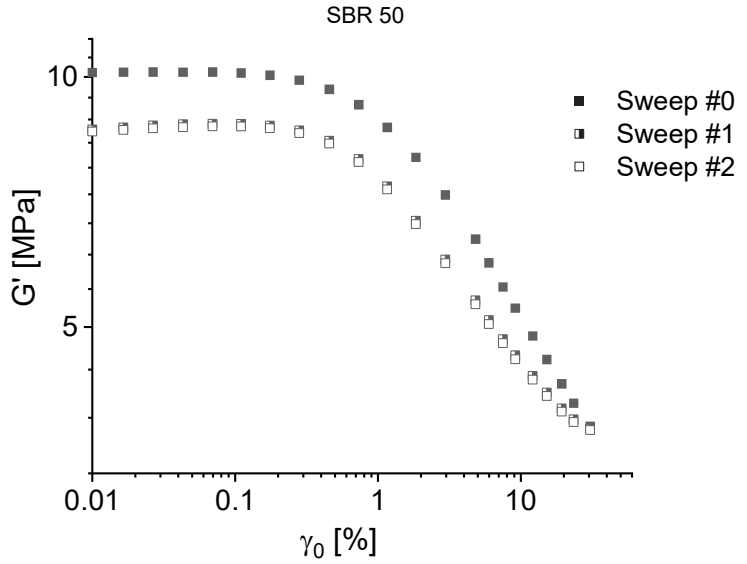

Figure 3.16. Zoom in on the storage modulus plot of SBR 50

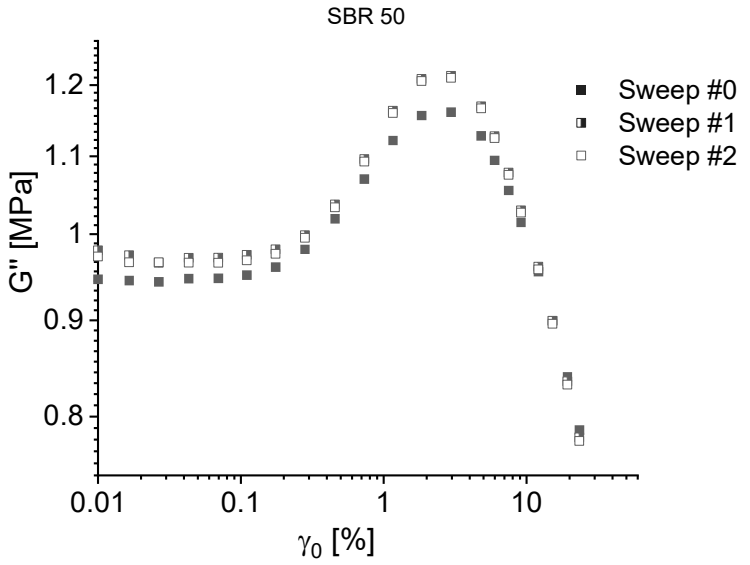

Figure 3.17. Zoom in on the loss modulus plot of SBR 50

The high strain amplitude region of the storage modulus also deserves close examination. Specifically, the initial #0 curve for SBR 50 and 75 phr silica rubber does not exhibit a second plateau, a feature that appears in the subsequent sweeps (Figure 3.14, Figure 3.16).

The observed second plateau may simply be a residual 'memory effect' from the previously applied maximum strain amplitude. The simplest way to assess this hypothesis is to add a subsequent amplitude sweep reaching amplitudes greater than 30%. Unfortunately, the instrument with this torsional setup has some problems going at higher amplitudes. The suggested procedure to verify it is to apply an amplitude

sweep from the linear regime to an amplitude which is in the middle of the G' softening. Then, after a rest time of tens of seconds, an additional amplitude sweep, which instead goes to higher amplitudes then before, should be applied. If at the intermediate amplitude of this second sweep the material would show a second plateau, it would be a suggestion that the second plateau seen in the present work could be apparent. Due to time reasons in this thesis work has been impossible to apply this additional experiment protocol.

Upon examining the loss modulus curves depicted in Figure 3.15 and Figure 3.17, it is noteworthy that the magnitude of the changes following sweep #0 is considerably less pronounced compared to the case of the storage modulus. Additionally, these changes in the loss modulus are accompanied by a noticeable increase in the peak values especially for SBR 50.

Given that filled rubbers are known to exhibit a time-dependent recovery effect after strain (1.4.3), the consistency of curves #1 and #2 suggest that the recovery kinetics remains unaffected by the amplitude sweep. This implies that the structural changes induced by the Payne effect do not alter the material's inherent (viscoelastic) recovery capabilities. Notably, this characteristic is observed regardless of filler content, rubber type, and frequency.

To confirm the independence of the above discussed feature on frequency, the ratios of G' and G'' measured at in the linear regime after the first amplitude sweep tests to those measured the second one were determined for each considered material (equations 3.1 and 3.2) and for each frequency, and then averaged.

$$\frac{G'_{0\#2}(\omega)}{G'_{0\#1}(\omega)} \qquad 3.1$$

$$\frac{G''_{0\#2}(\omega)}{G''_{0\#1}(\omega)} \qquad 3.2$$

The average is then reported along with the standard deviation as a function of filler content in Figure 3.18. The averages are based on a collective dataset derived from several samples, detailed samples' amount as follows: SBR 0 (13 samples), SBR 25 (12 samples), SBR 50 (12 samples), SBR 75 (13 samples), and NBR 60 (7 samples). The figures show that the average ratio is always 1, with a very small standard deviation, confirming that the above discussed feature is material and frequency insensitive.

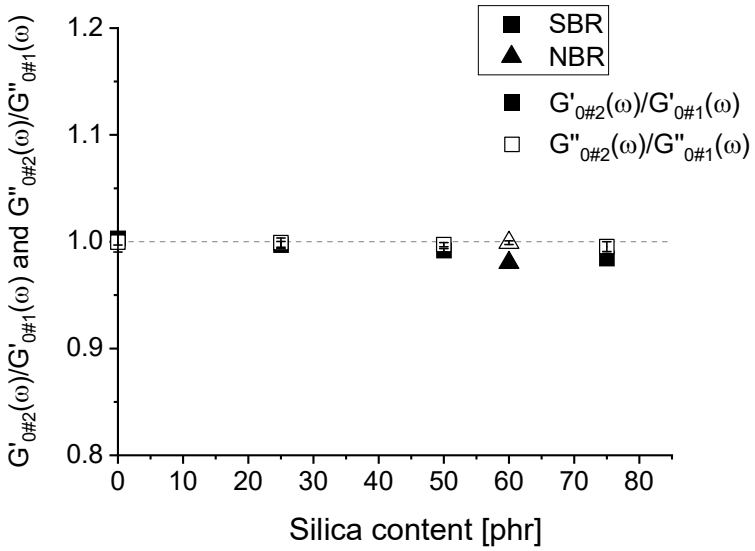

Figure 3.18 Ratios of the low amplitude storage moduli $G'_{0\#2}(\omega)\ /G'_{0\#1}(\omega)$ (full symbols) and loss moduli $G''_{0\#2}(\omega)/G''_{0\#1}(\omega)$ (empty symbols) versus the silica content

Structural variations: irreversibility assessment

The series of amplitudes brings evidence that only the virgin sample shows structural changes capable of altering the components of the dynamic moduli. It remains to be established whether these structural changes are irreversible, or if they only appear to be so due to a slow recovery process.

An indication that recovery is occurring can be deduced from variations in the successive frequency sweep tests protocol. Specifically, if the rest time between sweep #0 and #1 differs from that between #1 and #2, the material is likely to exhibit a greater G'_0 following the longer rest period. Here below an example of a sample of SBR 75 clearly shows this phenomenon (Figure 3.19).

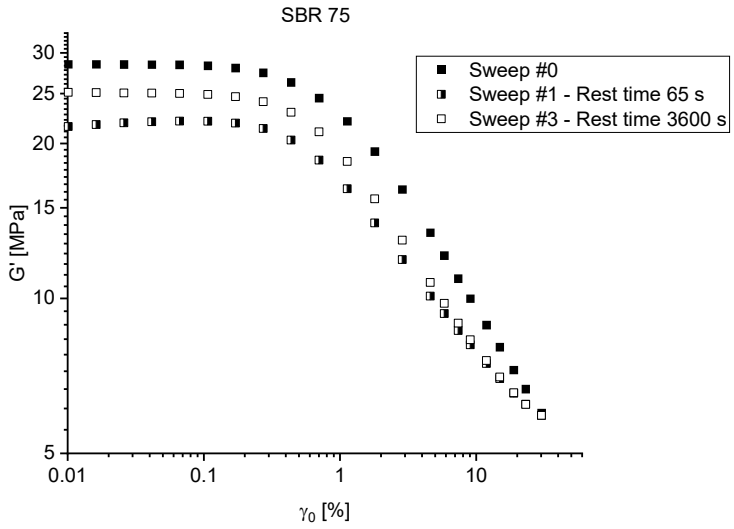

Figure 3.19. Graph present the storage modulus as a function of strain amplitude across different sweeps at 20 rad/s, illustrating the dependence of SBR 75 responses on rest time duration

An evidence supporting the idea that the effects of the structural change can be recovered, comes from observations made when the rest time between successive shear amplitude sweep tests is too short (Figure 3.20). In such cases, the material exhibits an increase in G' while increasing shear strain amplitude in the low amplitude region, were G'' is expected to be independent of shear strain amplitude; this phenomenon occurs only at low angular frequency, where the time required to get to the steady state and take the measurement is long. During this time a partial recovery of the structure may occur, leading to an increase of G' and decrease of G''.

When the measuring time is lower than the waiting time between two subsequent strain amplitude sweep tests, the apparent initial dependence of the viscoelastic properties on strain amplitude is not observed.

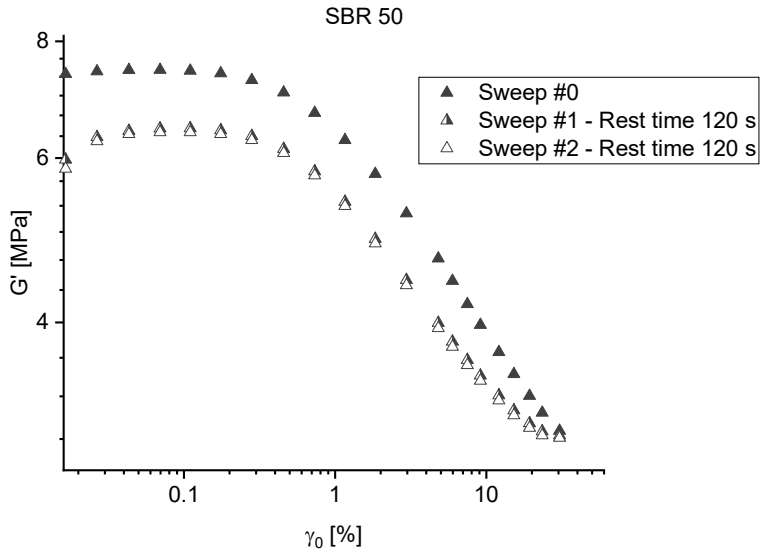

Figure 3.20. Graph presents the storage modulus as a function of strain amplitude across different sweeps at 0,1 rad/s, illustrating the dependence of SBR 50 responses on rest time duration

These preliminary findings and their implications motivated the following detailed analysis of the recovery of the value of G'_0 of the virgin material with time.

3.2.2. Recovery: series of strain amplitude sweep tests followed by a constant low strain amplitude test

Time effect on the low amplitude storage modulus

This section presents the experimental findings from the time recovery tests. Figure 3.21 illustrates the evolution of the storage modulus G' over time, without subjecting the data to further manipulation. This approach follows the groundwork laid by Luca Di Giosia [36], even though with a new analytical perspective focusing on whether the material can fully restore its low amplitude modulus before straining, $G'_{0\#0}$.

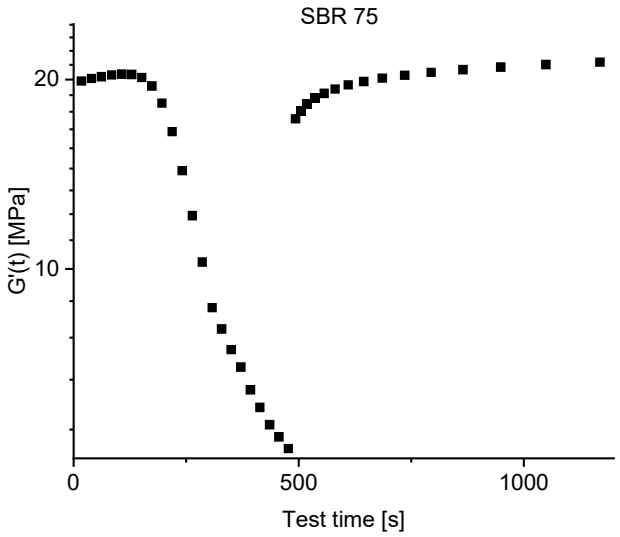

Figure 3.21. Graph depicting the results of G′ throughout the "sweep #2" and "recovery" phases over test time for SBR 75 at 5 rad/s

The plot displays the relationship between G', and the elapsed test time for an SBR 75 sample at 5 rad/s. Initially, the graph depicts an increase in strain amplitude during the 500s third shear strain amplitude sweep where the Payne effect is observable. Subsequently, $G'_{0\#3}(t)$ recovery is monitored under the application of a constant low shear strain amplitude. For this experiment, the monitoring period for $G'_{0\#3}(t)$ spans several decades. However, the time scales generally used in these analyses vary, extending to 10^3 s, 10^4 s, and even 10^5 s.

The focus now shifts to the right-hand portion of the graph to investigate whether the material regains its original linear modulus. This is achieved by calculating the ratio of the monitored modulus over time ($G'_{0\#3}(t)$) to the pristine linear modulus $G'_{0\#0}$, Eq. 3.3. This representation is advantageous not only because it charts the initial loss and eventual recovery to the virgin modulus (a ratio of 1 indicating full recovery), but also because it theoretically eliminates the influence of frequency dependency on the low amplitude modulus, resulting in a more consistent comparison across frequencies. Figure 3.22, using this normalized approach, effectively compares the recovery kinetics of all materials while accounting for frequency-related variability.

$$\frac{G'_{0\#3}(t)}{G'_{0\#0}} \qquad 3.3$$

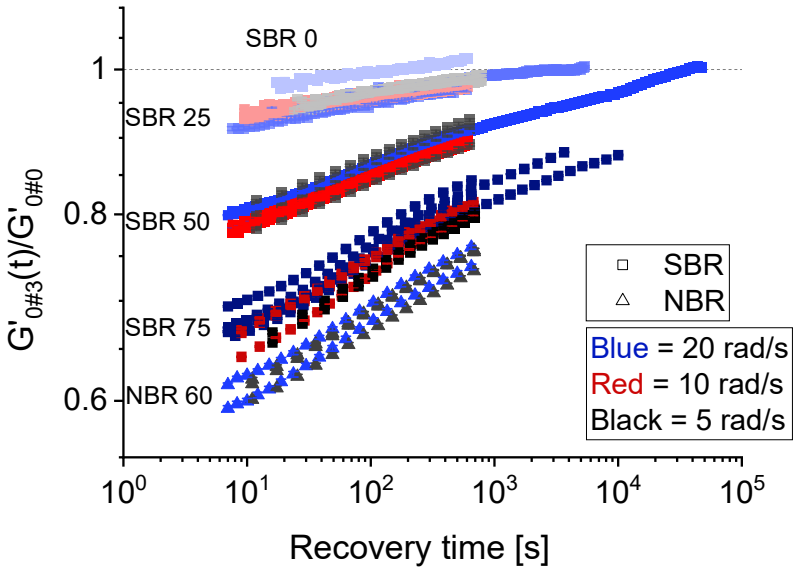

Figure 3.22. $G'_{0\#3}(t)/G'_{0\#0}$ time dependence in a double logarithmic plot, depicting the recovery kinetics of different materials (squares for SBR with varying silica content levels indicated by transparency; triangles for NBR) and frequencies (black for 5 rad/s, red for 10 rad/s, blue for 20 rad/s)

Figure 3.22, employing a double logarithmic scale, effectively illustrates the recovery process across various materials. The graph collects data from multiple samples tested at different frequencies. Notably, the SBR 50 sample, subjected to a constant strain amplitude over a timescale of 10^5 s, approaches a ratio close to 1, suggesting a full recovery of its virgin low amplitude storage modulus.

It's interesting to highlight that the SBR samples with no silica also exhibit an increase in modulus. However, this increase couldn't be related to a recovery of the Payne effect but is likely attributable to viscoelastic recovery from the previous extensive strain. For the SBR 0 phr sample, the slightly above one values could be attributed to instrument sensitivity limits and additionally to the fact that taking a ratio between to experimental values, amplifies the measurement error in. An additional explanation could be that the energy imparted by the deformation history might promote the progression of the crosslinking process. However, this needs to be further explored through subsequent analyses on the same specimen.

Regarding frequency effects, there is no consistent pattern observable; actually, curves at different frequencies counterintuitively in some cases (SBR 50, 75 and NBR 60) higher frequency curves are contained among the lower frequency ones. This fact possibly is due sample variability, potentially in silica dispersion among samples.

The rate at which materials recover varies significantly with the filler content. The curves seem to have a slight sigmoidal trend. A simple, fast but not fully correct way to contrast these kinetic properties could be fitting the ratio values $G'_{0\#3}(t)/G'_{0\#0}$ (Figure 3.22) with a power law function, as equation (3.4a, which become a linear function on the double logarithmic scale (equation (3.5b).

$$f(x) = ax^b \tag{3.4a}$$

$$\log\big(f(x)\big) = b\log(x) + \log(a) \tag{3.5b}$$

In order to minimize the error incurred when using this function to fit the curves, only data from the start of the curves up to approximately 600 seconds are considered. The "b" parameter, shown in Figure 3.23 in relation to silica content, is the slope of the linear fitting function on a double logarithmic scale. This parameter qualitatively characterizes the recovery kinetics of the materials.

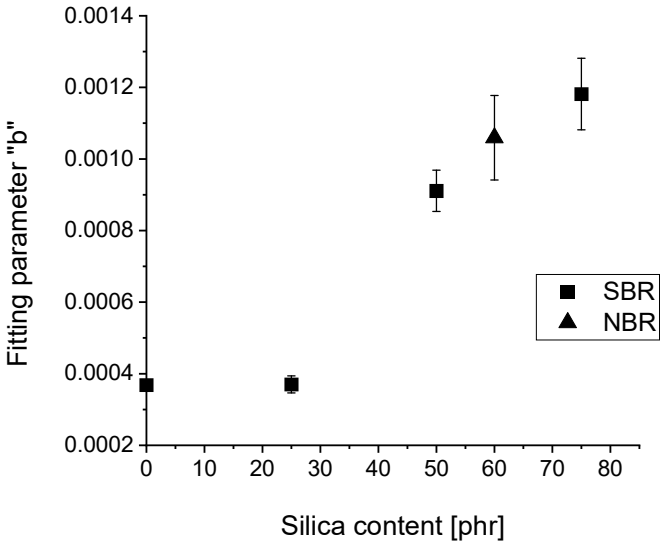

Figure 3.23. The graph displays the slope derived from the linear interpolation of $G'_{0\#3}(t)/G'_{0\#0}$ versus time on a double logarithmic scale, plotted as a function of filler content

To extend the time scale of observation for the low amplitude modulus recovery in SBR 50 and 75 materials, a selection of samples was removed from the testing apparatus at the conclusion of the initial recovery test. These samples were stored and then, after an interval of approximately one week or one month, tested again by applying a constant low strain amplitude. Figure 3.25 and Figure 3.24 presents the

result in terms of ratio (Equation 3.3). The error bars included account for the maximum error introduced by positioning and clamping (as discussed in 2.4).

Notably, these later measurements also register ratios exceeding the unit value, suggesting an "over-recovery". Indeed, the difference may be partly explained with measurement errors (and their combination in considering the ratio of experimental values), and partly with the different temperatures in the lab between the two measurement sessions. Starting from the modulus increase, to reinforce this hypothesis one could estimate the necessary temperature variation using the molecular theory of elasticity. Unfortunately the density of crosslinking is not known for these materials, so further investigations about it are needed.

Nevertheless, these supplementary data points lend weight to the assertion that the low amplitude modulus of virgin materials can be fully restored, provided sufficient rest time is allowed. This finding demonstrates that the structural changes of the materials induced by the Payne effect have reversible nature, even if the recovery kinetic is quite slow.

Previously, it has been shown that amplitude sweeps do not significantly impact recovery kinetics. Therefore, even though the current results on recovery are derived after a sequence of amplitude sweeps, it is logical to assume that they would also apply to specimens subjected to a single strain, given this evidence.

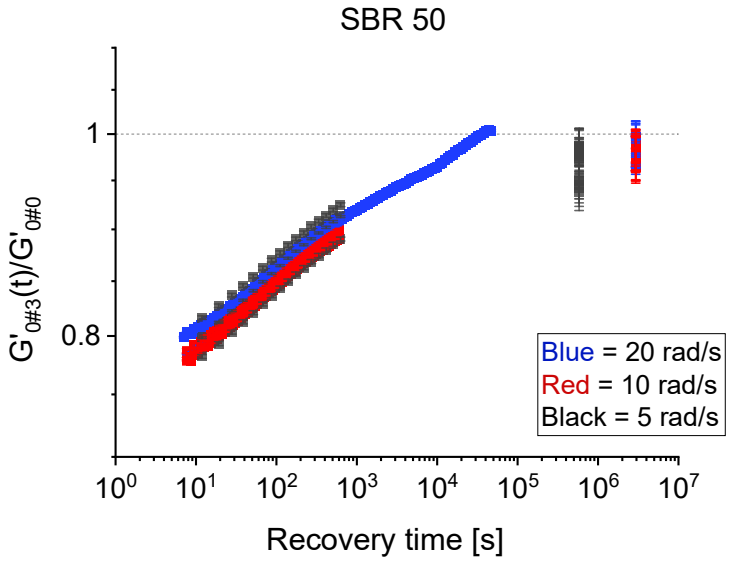

Figure 3.24. Double logarithmic plot of SBR 50's $G'_{0\#3}(t)/G'_{0\#0}$ over diverse time scales and frequencies, featuring additional data points collected after approximately one week and one month (10^6 seconds)

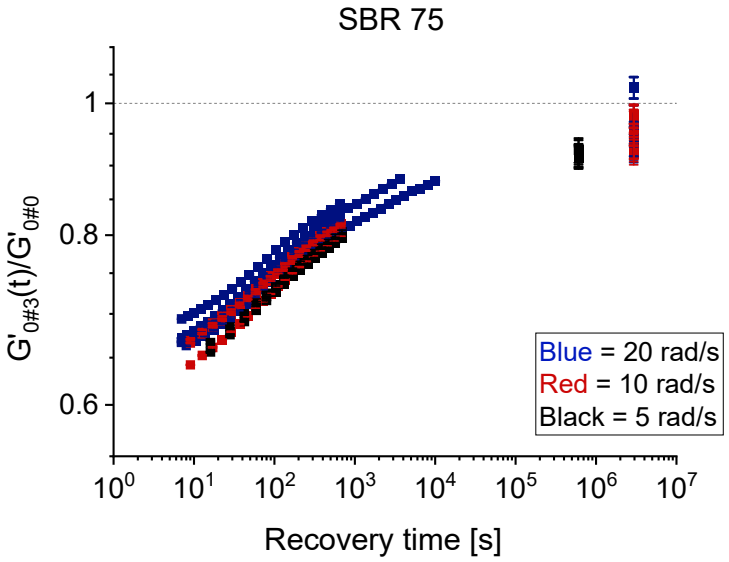

Figure 3.25. Double logarithmic plot of SBR 75's $G'_{0\#3}(t)/G'_{0\#0}$ over diverse time scales and frequencies, featuring additional data points collected after approximately one month (10^6 s)

Time effect on the storage modulus in high strain amplitude region

The difference between the response to shear strain amplitude sweeps on the virgin material (sweep #0) and the strained one (sweep #1) has been previously established and is characterized by two main features. The first is the reduction of the low amplitude storage modulus, G′$_0$, extensively discussed and analyzed in a prior paragraph. The second refers to the shape of the tail end of the curve, whose shape suggests the existence of a second plateau. Furthermore, although less pronounced, there are also changes observed in the loss modulus.

Above, the possibility to recover the unstrained material small strain elastic component of the modulus, $G'_{0\#0}$ has been discussed. Now the shape of the response to shear strain amplitude sweep tests of the material after recovery will be considered in terms of both G′ and G′′. The method to investigate the recovery of the curve's original shape involved conducting an amplitude sweep after the series of amplitude sweeps, with variable resting periods, without the removal of the samples, are described at the end of the section 2.2.4. Due to time constraints in the thesis work, the test was only conducted on SBR 50 and 75 at a frequency of 20 rad/s. The experimental outcomes for SBR 75 are represented in subsequent figures (Figure 3.26, Figure 3.27, Figure 3.28, Figure 3.29), each showcasing the sweep #0 curve to represent the response of the virgin specimen, juxtaposed with the sweep #1 and sweep #2 curve to visually compare the changes in curve shape. It is useful to remember that sweep#1 and sweep#2 curves were shown to overlap when the same rest time is waited before each of the two shear strain amplitude sweep tests, while in this experiment the rest time between sweeps is varied to capture “snapshots” of the recovery at different recovery phases.

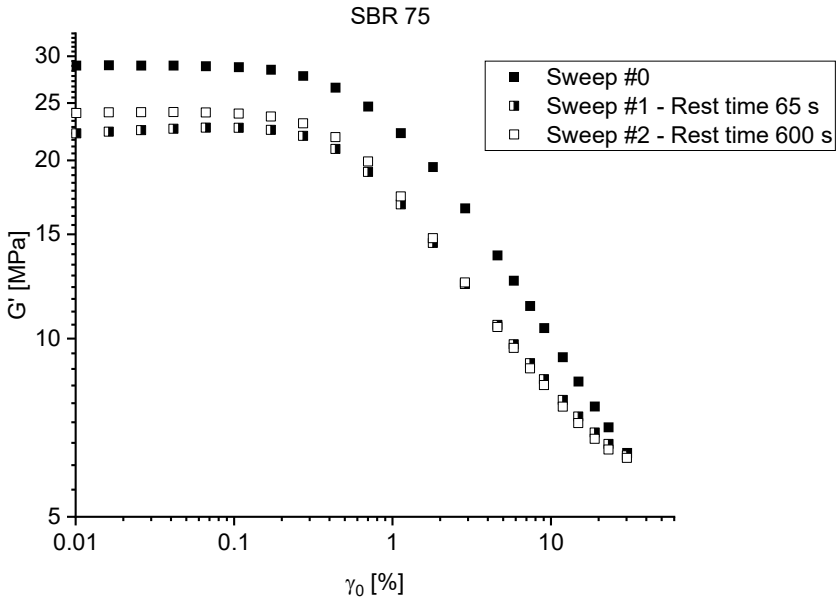

Figure 3.26. Storage modulus for subsequent amplitude sweeps for SBR 75 at 20 rad/s are represented, the rest time between #0 and #1 is equal to 65 s instead between sweeps #1 and #2 the sample rest for 600 s

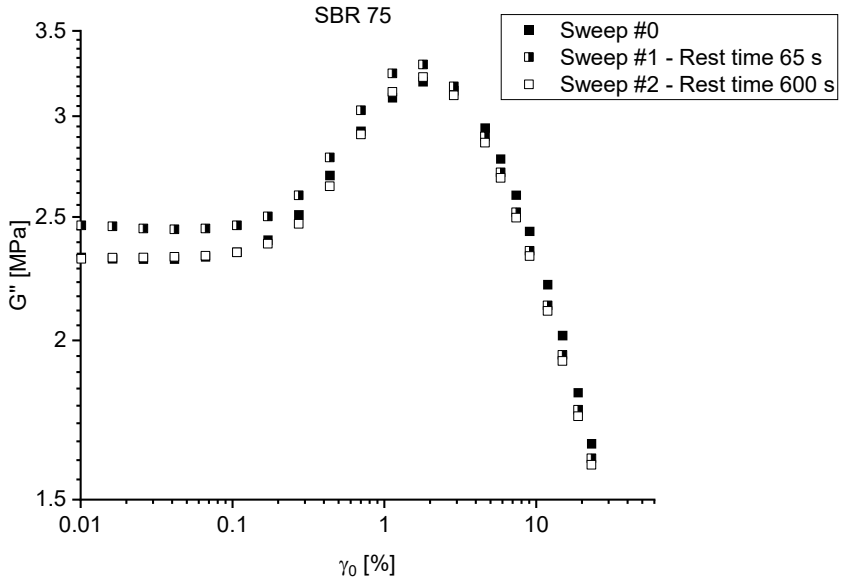

Figure 3.27. Loss modulus for subsequent amplitude sweeps for SBR 75 at 20 rad/s are represented, the rest time between #0 and #1 is equal to 65 s instead between sweeps #1 and #2 the sample rest for 600 s

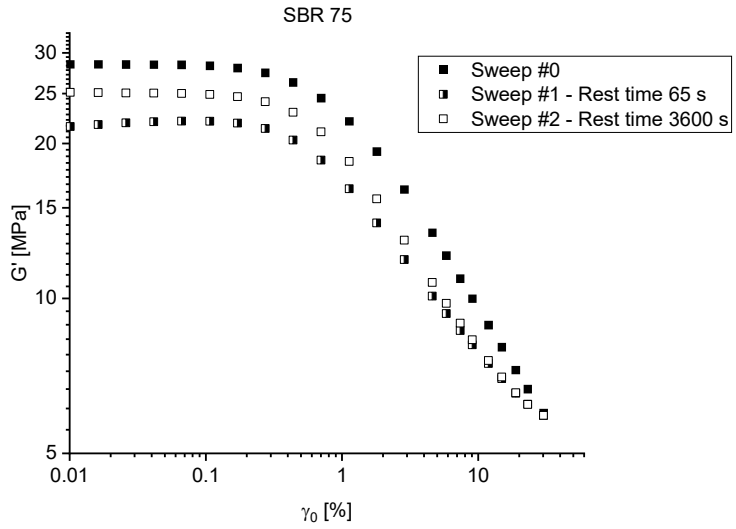

Figure 3.28. Storage modulus for subsequent amplitude sweeps for SBR 75 at 20 rad/s are represented, the rest time between #0 and #1 is equal to 65 s instead between sweeps #1 and #2 the sample rest for 3600 s

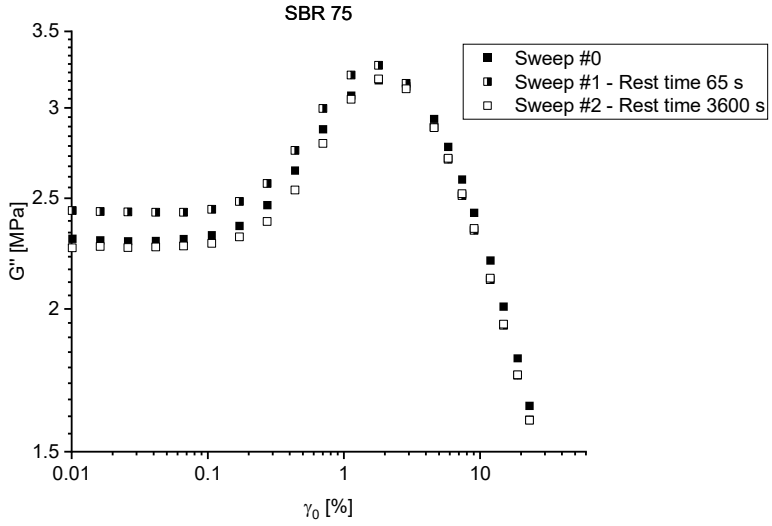

Figure 3.29. Loss modulus for subsequent amplitude sweeps for SBR 75 at 20 rad/s are represented, the rest time between #0 and #1 is equal to 65 s instead between sweeps #1 and #2 the sample rest for 3600 s

The data reveal that even specimens that nearly fully recovered the low amplitude modulus still exhibit a different response in the high strain amplitude domain with respect to the unstrained material (sweep #0). This could be due to one of two factors: either the necessary rest period for complete recovery of the original characteristics is

more extended, or the high strain amplitude changes are related to the irreversible Mullins effect. Because of the slow kinetics, analyzing the full recovery of SBR 75 while leaving the sample in place could be challenging. Consequently, SBR 50 was also examined with a second rest period of 50400 seconds (Figure 3.30 and Figure 3.31).

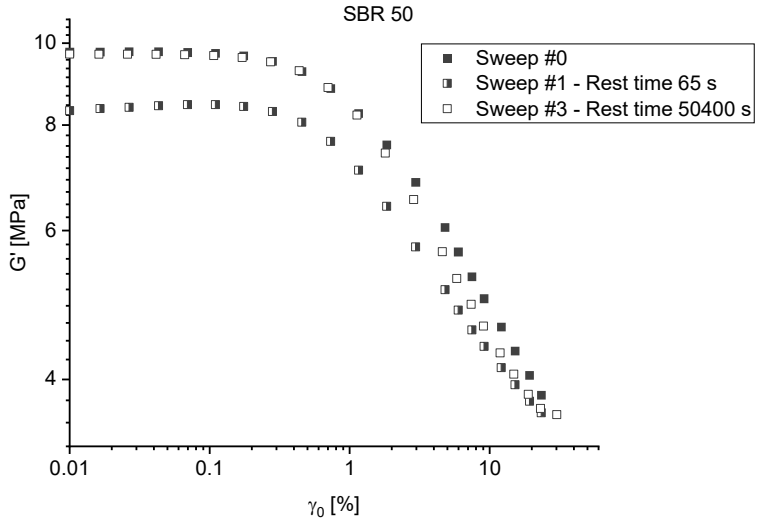

Figure 3.30. Storage modulus for subsequent amplitude sweeps for SBR 50 at 20 rad/s are represented, the rest time between #0 and #1 is equal to 65 s instead between sweeps #1 and #2 the sample rest for 50400 s

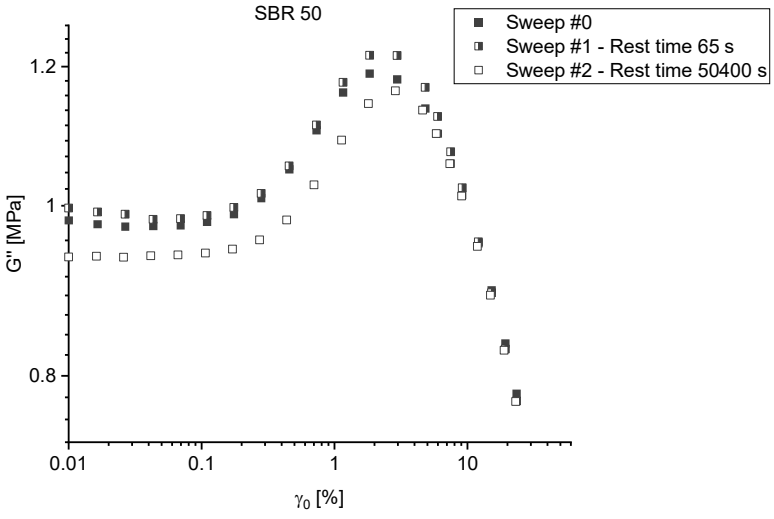

Figure 3.31. Loss modulus for subsequent amplitude sweeps for SBR 50 at 20 rad/s are represented, the rest time between #0 and #1 is equal to 65 s instead between sweeps #1 and #2 the sample rest for 50400 s

Unfortunately, the loss modulus of SBR 50 exhibits unexpected vertical shifts (Figures). Notably, the low amplitude modulus of sweep #2 falls below the pristine property. This unusual behavior warrants additional investigation in future studies to determine if it is merely a result of measurement system noise. On the other hand, the G' curves show the recovery of the initial plateau G'_0, yet they do not completely restore the initial response shape of sweep #0 at high amplitudes (Figure).

In other to further investigate the initial reversibility hypothesis on a higher time scale, the same samples just analyzed were removed from the rheometer setup and subsequently stored for one month to allow recovery. Then they were subjected to an additional amplitude sweep, identified here as sweep #3. The data gathered from this procedure are illustrated in the Figure 3.34 and Figure 3.32.

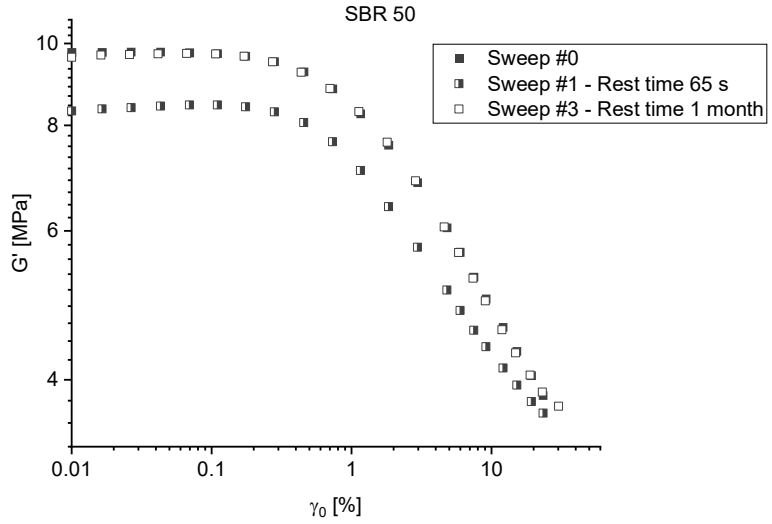

Figure 3.32. Representation of the storage modulus for SBR 50 at 20 rad/s across consecutive amplitude sweeps. Post-sweep #2, which is not depicted to make the graph clearer, the sample was set aside and subsequently retested to execute sweep #3 following a rest period of one month

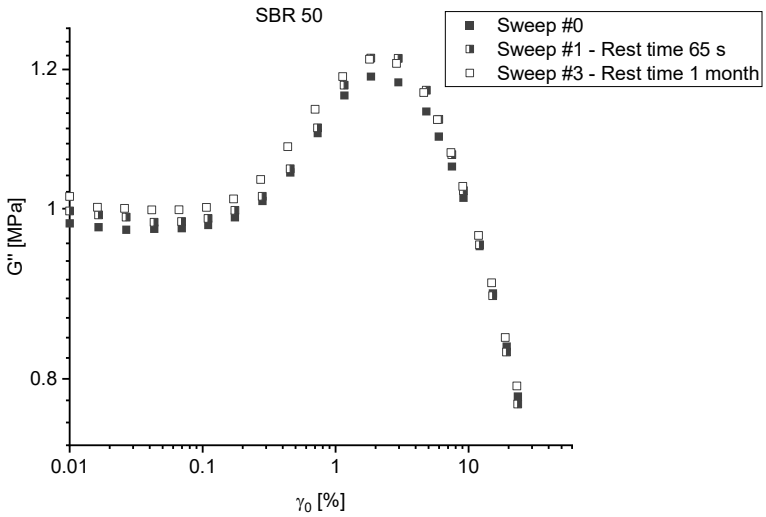

Figure 3.33. Representation of the loss modulus for SBR 50 at 20 rad/s across consecutive amplitude sweeps. Post-sweep #2, which is not depicted to make the graph clearer, the sample was set aside and subsequently retested to execute sweep #3 following a rest period of one month

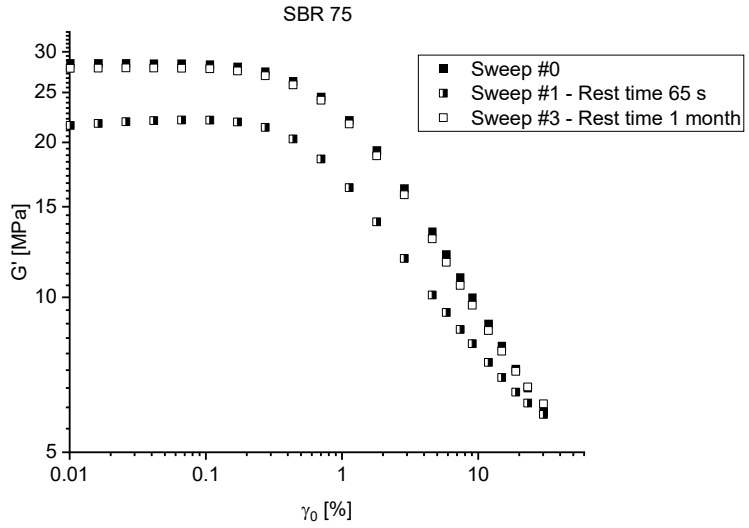

Figure 3.34. Representation of the storage modulus for SBR 75 at 20 rad/s across consecutive amplitude sweeps. Post-sweep #2, which is not depicted to make the graph clearer, the sample was set aside and subsequently retested to execute sweep #3 following a rest period of one month

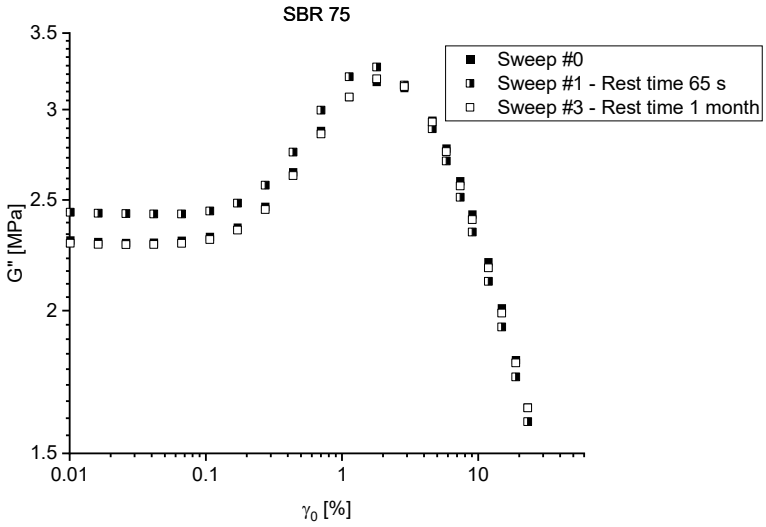

Figure 3.35. Representation of the loss modulus for SBR 75 at 20 rad/s across consecutive amplitude sweeps. Post-sweep #2, which is not depicted to make the graph clearer, the sample was set aside and subsequently retested to execute sweep #3 following a rest period of one month

The almost complete overlap of sweep #3 curves of G' and G'' with the initial sweep #0 indicates that SBR 50 and 75 experience predominantly reversible structural modifications through the course of strain amplitude testing history. Any potential irreversible small changes, if present, do not seem to affect the Payne effect curve after recovery.

3.3. Frequency effect

The experimental data have been considered also to investigate the impact of frequency on the Payne effect. Notably, frequency's influence on the shape of the dynamic moduli as a function of shear strain amplitude appears negligible, as established in literature [29] [30]. This phenomenon is referred to as "frequency-insensitive feature of the Payne effect." Li et al. in 2017 observes this across various rubbers and filler types over a broad frequency range (0.004 – 10 Hz), and indicates that filled rubbers tested by shear strain amplitude sweep at different frequencies exhibit merely vertical shifts in their moduli (in a logarithmic scale), correlating with frequency changes.

This phenomenon implies the separability of amplitude and frequency effects on dynamic modulus components, a concept mathematically represented by Li (2017) in equation 1.8.

The current chapter aims to validate this feature in the studied system. An initial investigation focused on the low amplitude modulus's frequency dependence (0,01%

strain amplitudes) through frequency sweep tests (0,1-20 rad/s). The results, presented in Figure 3.36 and Figure 3.37 in double logarithmic scale, reveal a moderate dependency of the low amplitude moduli on frequency, with moduli at most doubling over a three-order frequency magnitude increase.

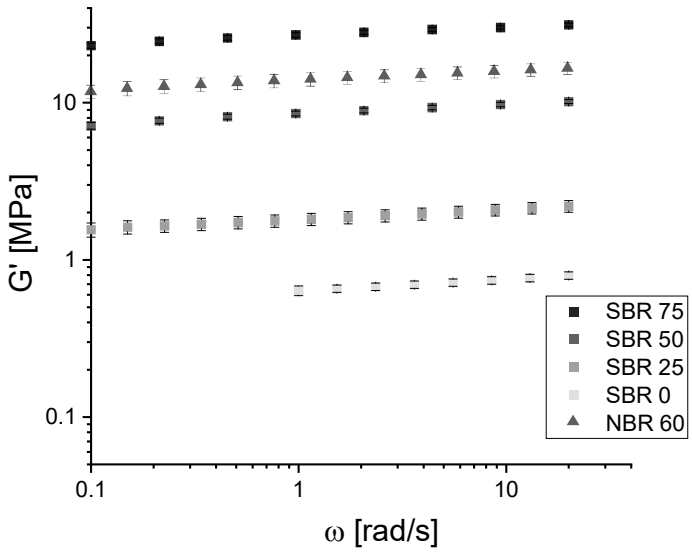

Figure 3.36. The storage component of the dynamic modulus in function of the frequency for filled and unfilled rubbers, where the content of filler is differentiated by the grey scales and the rubbers by squared (SBR) and triangular (NBR) symbols

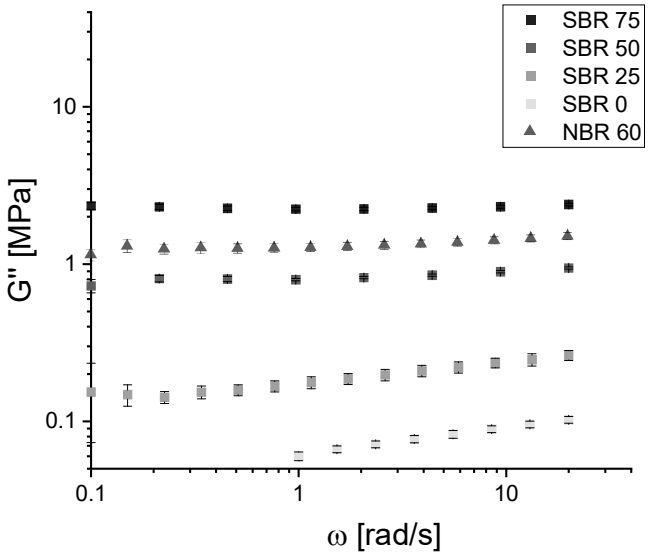

Figure 3.37. The loss component of the dynamic modulus in function of the frequency for filled and unfilled rubbers, where the content of filler is differentiated by the grey scales and the rubbers by squared (SBR) and triangular (NBR) symbols

Further tests involved shear strain amplitude sweeps (Section 2.2.3) at logarithmically increasing strain amplitudes (γ_0 0,01-30%) across various frequencies (0,1-1-5-10-20 rad/s). The outcomes of these tests are presented from Figure 3.44 to Figure 3.47.

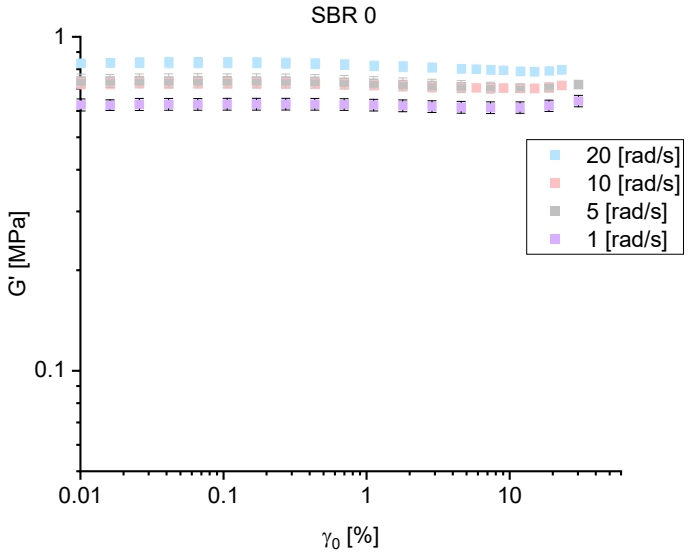

Figure 3.38. The SBR 0's storage modulus in function of the strain amplitude for different frequencies 1, 5, 10 and 20 rad/s represented by different colors: purple, grey, pink, blue respectively

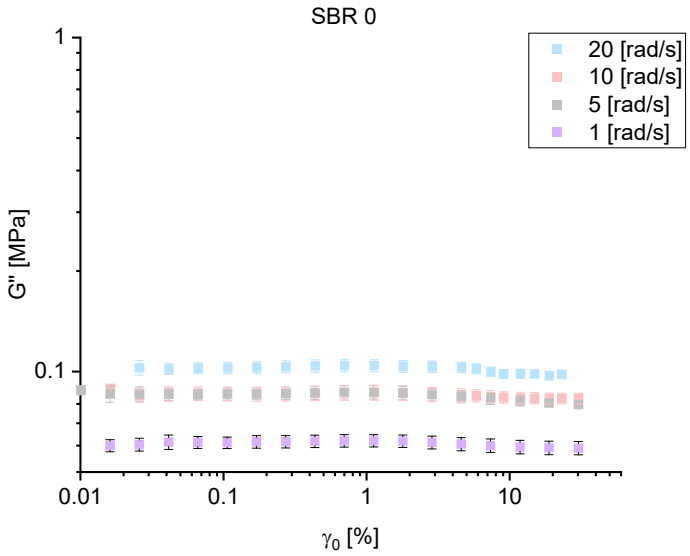

Figure 3.39. The SBR 0's loss modulus in function of the strain amplitude for different frequencies 1, 5, 10 and 20 rad/s represented by different colors: purple, grey, pink, blue respectively

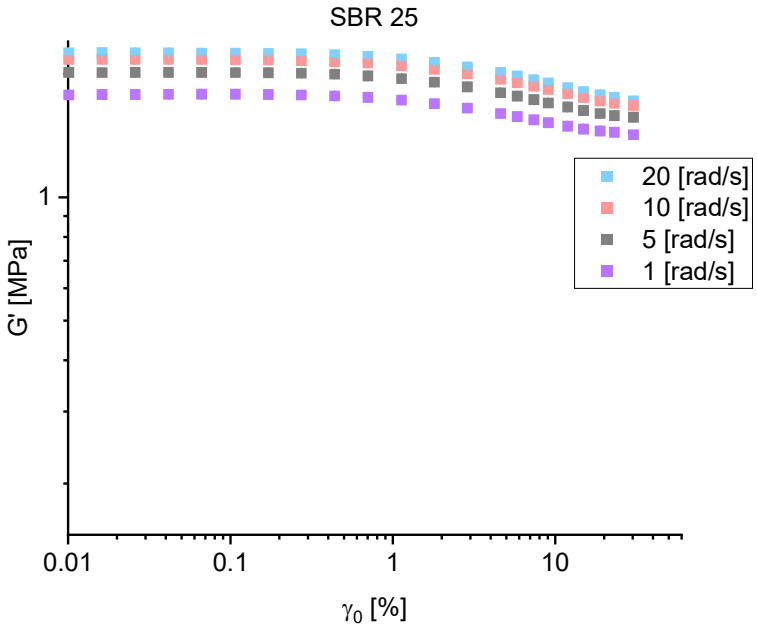

Figure 3.40. The SBR 25's storage modulus in function of the strain amplitude for different frequencies 1, 5, 10 and 20 rad/s represented by different colors: purple, grey, pink, blue respectively

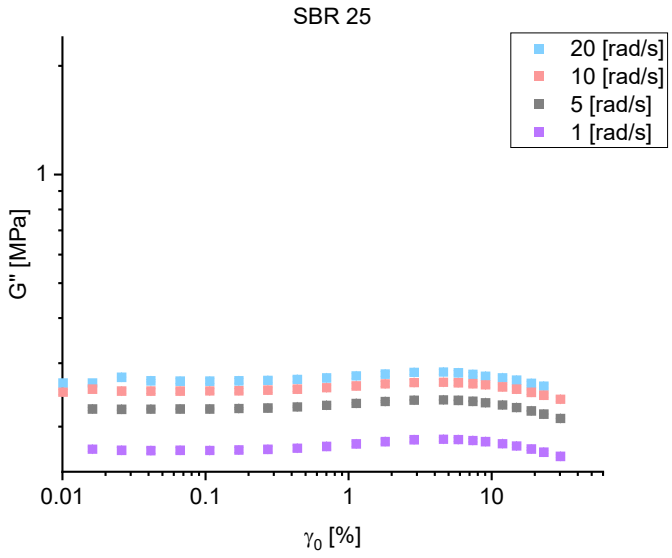

Figure 3.41. The SBR 25's loss modulus in function of the strain amplitude for different frequencies 1, 5, 10 and 20 rad/s represented by different colors: purple, grey, pink, blue respectively

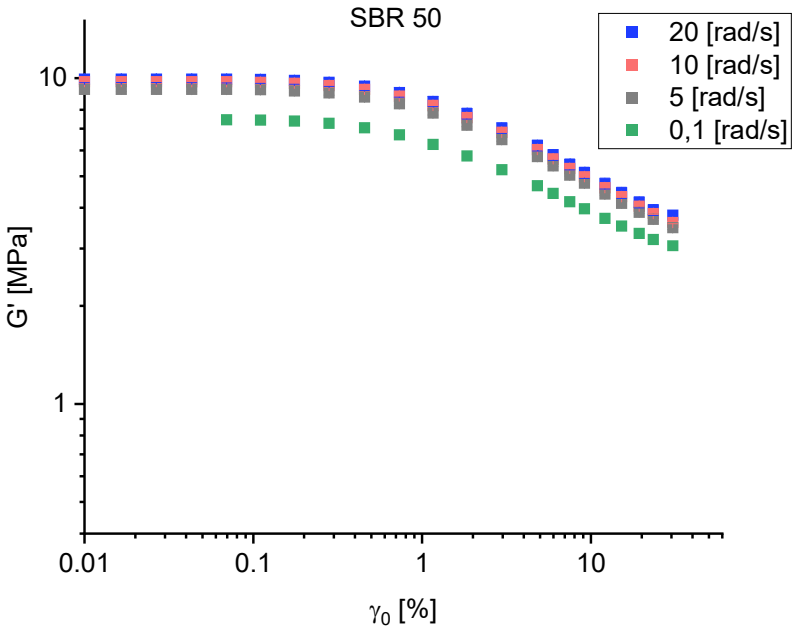

Figure 3.42. The SBR 50's storage modulus in function of the strain amplitude for different frequencies 0,1, 5, 10 and 20 rad/s represented by different colors: green, grey, pink, blue respectively

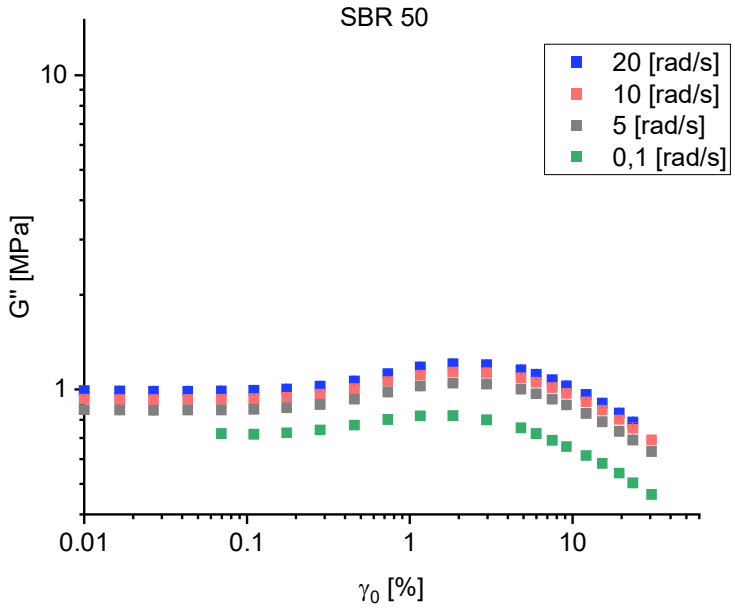

Figure 3.43. The SBR 50's loss modulus in function of the strain amplitude for different frequencies 0,1, 5, 10 and 20 rad/s represented by different colors: green, grey, pink, blue respectively

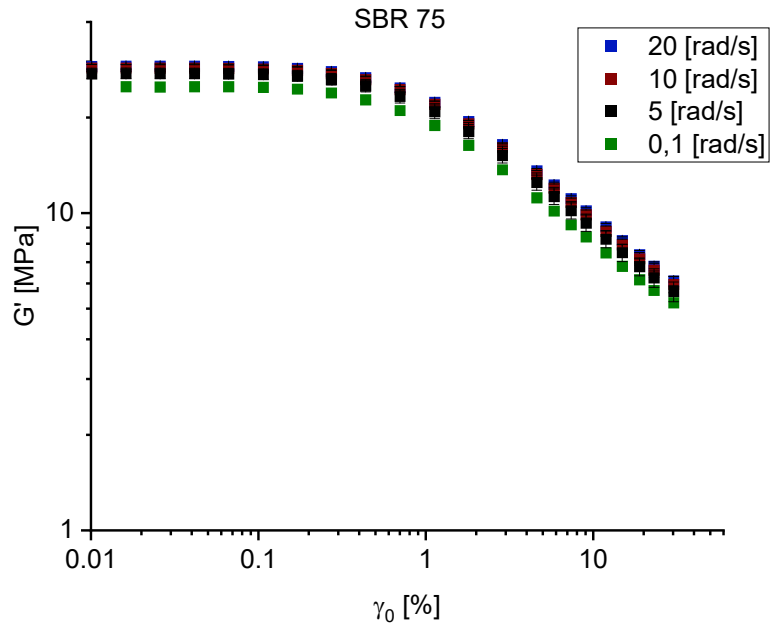

Figure 3.44. The SBR 75's storage modulus in function of the strain amplitude for different frequencies 0,1, 5, 10 and 20 rad/s represented with different colors: green, black, dark red, blue respectively

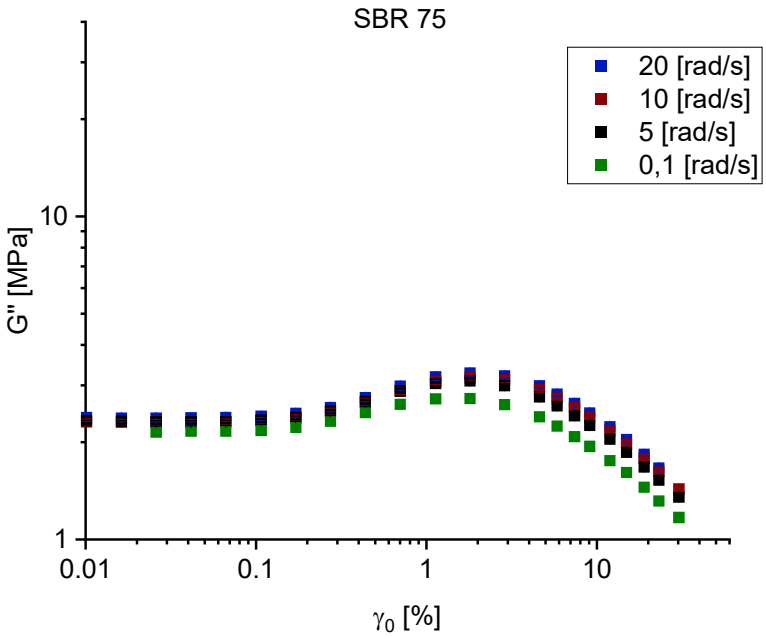

Figure 3.45. The SBR 75's loss modulus in function of the strain amplitude for different frequencies 0,1, 5, 10 and 20 rad/s represented with different colors: green, black, dark red, blue respectively

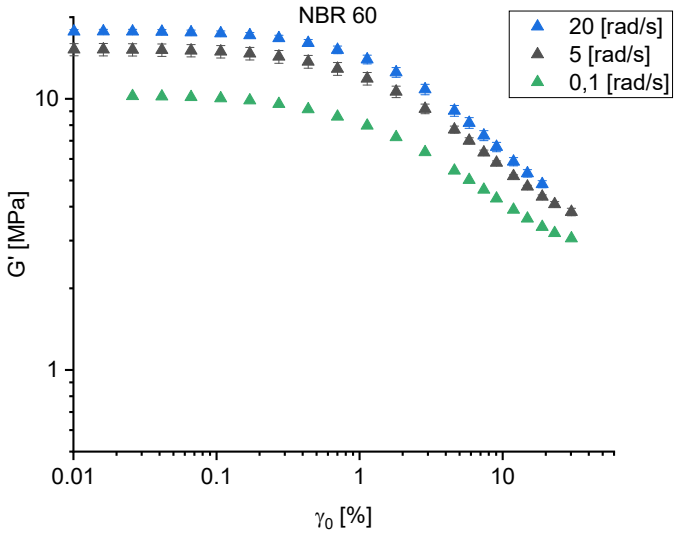

Figure 3.46. The NBR 60's storage modulus in function of the strain amplitude for different frequencies 0,1, 5 and 20 rad/s represented by different colors: green, grey, and blue respectively

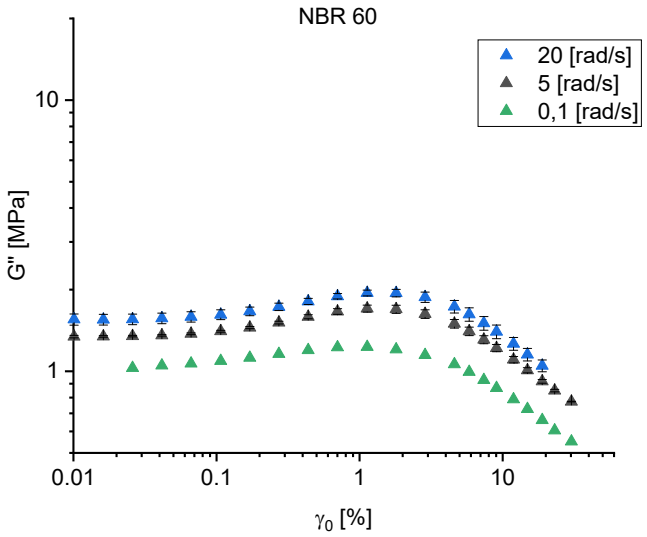

Figure 3.47. The NBR 60's loss modulus in function of the strain amplitude for different frequencies 0,1, 5 and 20 rad/s represented by different colors: green, grey, and blue respectively

These results indicate a vertical shift in the moduli values. To determine whether this shift is uniform across all applied strain amplitudes, Li (2017) recommends a method of normalization. This involves normalizing the components of the dynamic modulus by their corresponding low amplitude values, as in equation 3.6:

$$\begin{cases} \dfrac{G'(\gamma_0,\omega)}{G'_0(\omega)} = f(\gamma_0) \\ \dfrac{G''(\gamma_0,\omega)}{G''_0(\omega)} = g(\gamma_0) \end{cases} \qquad 3.6$$

If the frequency does not impact the amplitude dependence, the curves, once normalized, would overlap. The elaborated data are reported in the following graphs (from Figure 3.54 to Figure 3.57).

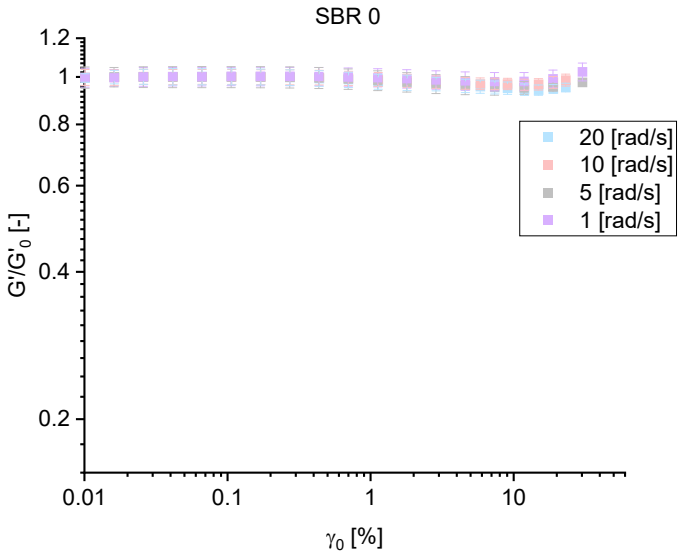

Figure 3.48. The normalized shear storage modulus for SBR 0 in function of the shear strain amplitude

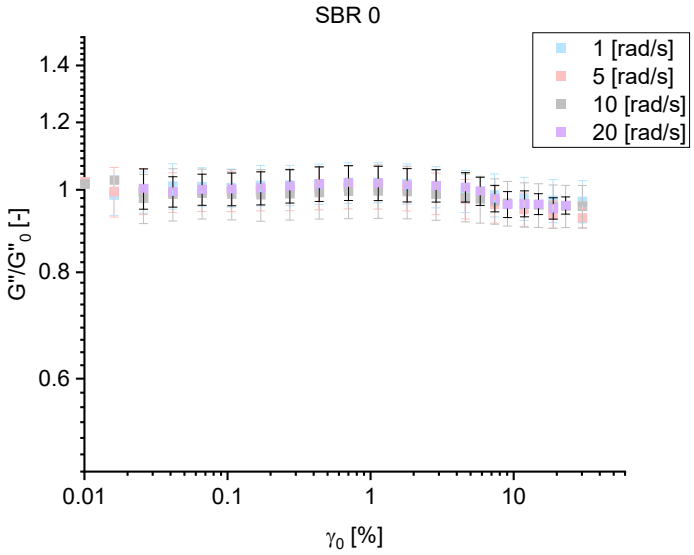

Figure 3.49. The normalized shear loss modulus for SBR 0 in function of the shear strain amplitude

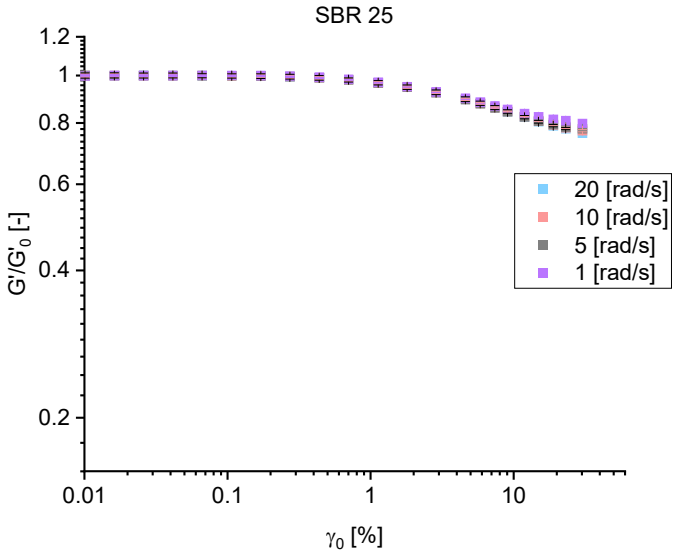

Figure 3.50. The normalized shear storage modulus for SBR 25 in function of the shear strain amplitude

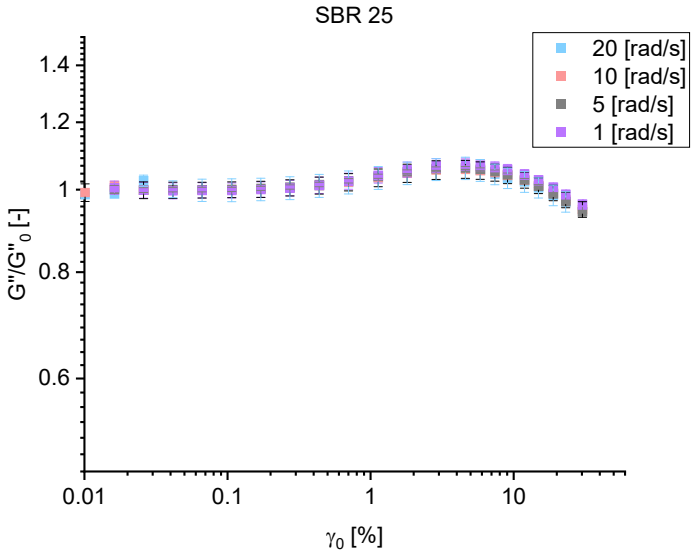

Figure 3.51. The normalized shear loss modulus for SBR 25 in function of the shear strain amplitude

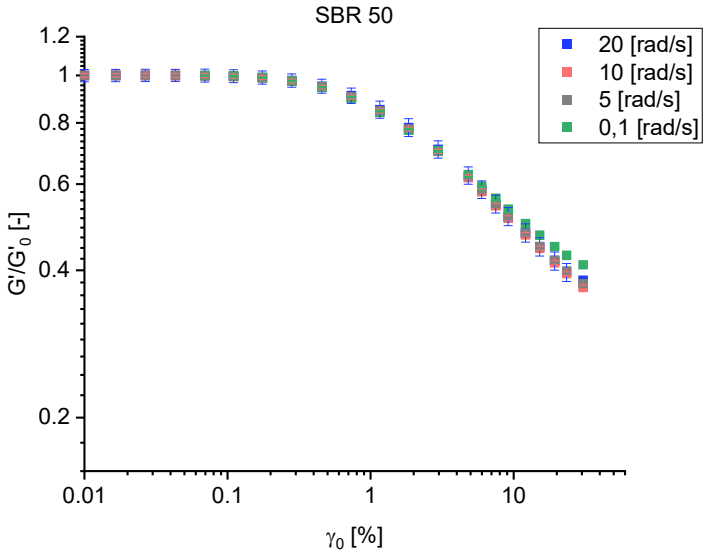

Figure 3.52. The normalized shear storage modulus for SBR 50 in function of the shear strain amplitude

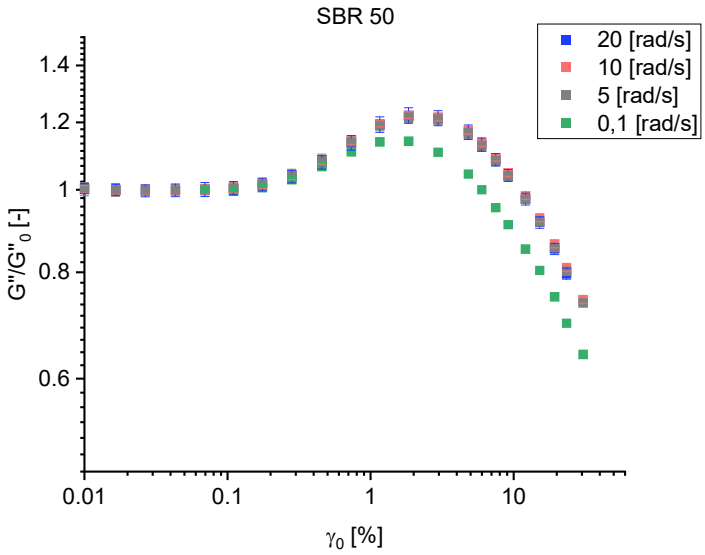

Figure 3.53. The normalized shear loss modulus for SBR 50 in function of the shear strain amplitude

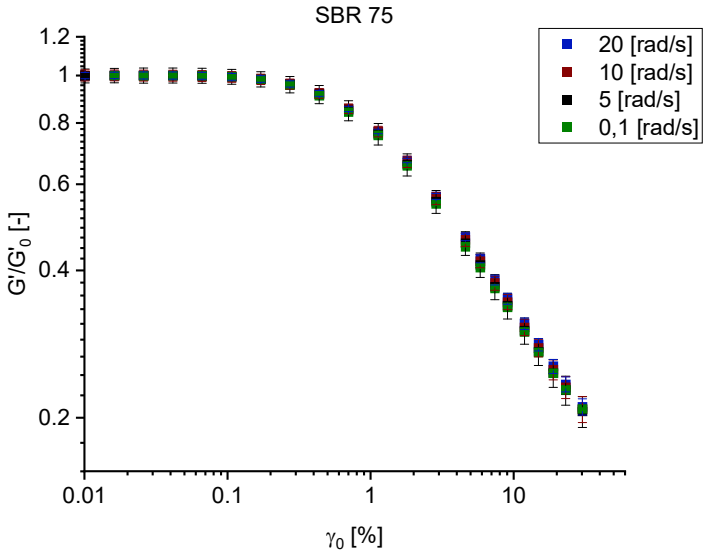

Figure 3.54. The normalized shear storage modulus for SBR 75 in function of the shear strain amplitude

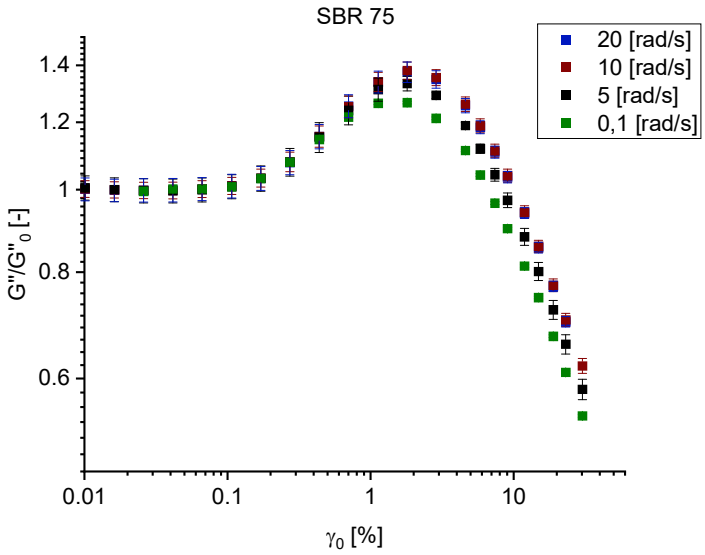

Figure 3.55. The normalized shear loss modulus for SBR 75 in function of the shear strain amplitude

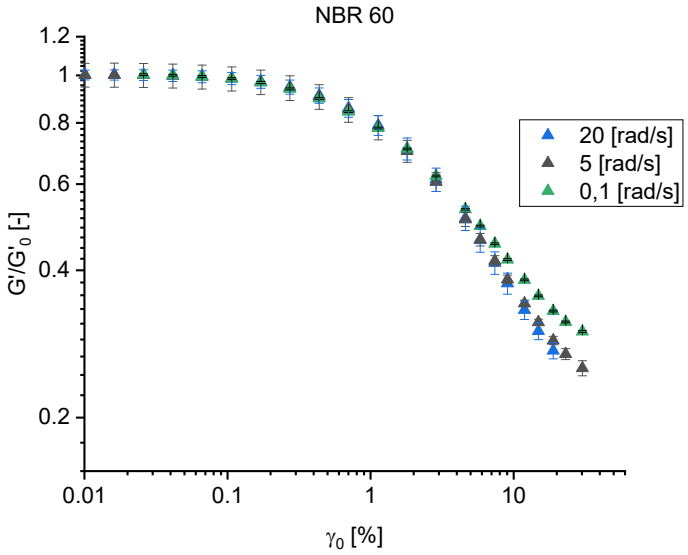

Figure 3.56. The normalized shear storage modulus for NBR 60 in function of the shear strain amplitude

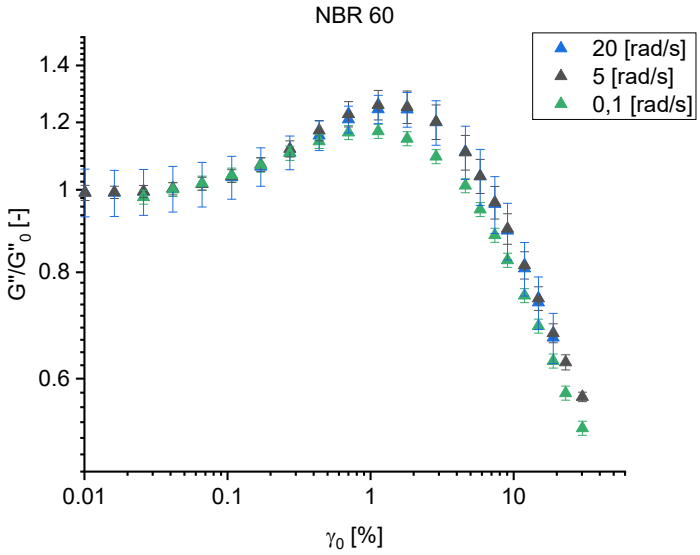

Figure 3.57. The normalized shear loss modulus for NBR 60 in function of the shear strain amplitude

The analysis reveals that for the case of SBR 75, SBR 50 and NBR 60 curves at the lower frequencies (0,1 and 5 rad/s) do not fully overlap, suggesting that the amplitude-frequency separability does not apply to their dissipative behavior at low frequencies. This is particularly evident in the loss modulus curves, at medium to high shear strain amplitudes.

The increased storage modulus ratio at higher amplitudes could be due to the emergence of higher harmonics, which could impact the separability of frequency and amplitude. The analysis of the loss modulus data indicates that at lower frequencies, there is less dissipative movement in the molecules compared to higher frequencies. This could be attributed to partial recovery during tests, but this factor seems to be not as impactful for the loss modulus. Alternatively, a more plausible explanation is that these materials undergo different deformation mechanisms at lower frequencies, possibly involving reduced molecular desorption from the silica particles' surface, given the extended time available for molecules to adjust to the applied shear strains.

However, due to time constraints, it was not possible to check the same phenomenon for SBR 0 and 25 lack at 0,1 rad/s, though the overlap in the available frequency range is satisfactory.

Normalization also facilitates the comparison of how different materials behave as the amplitude increases. Figure 3.58 showcases the variations in the storage and loss moduli at the highest shear strain amplitude applied (30%) specifically in relation to silica content.

$$\begin{cases} \dfrac{G'_{\gamma_0=0.30}(\omega)}{G'_0(\omega)} \\ \dfrac{G''_{\gamma_0=0.30}(\omega)}{G''_0(\omega)} \end{cases} \qquad 1.10$$

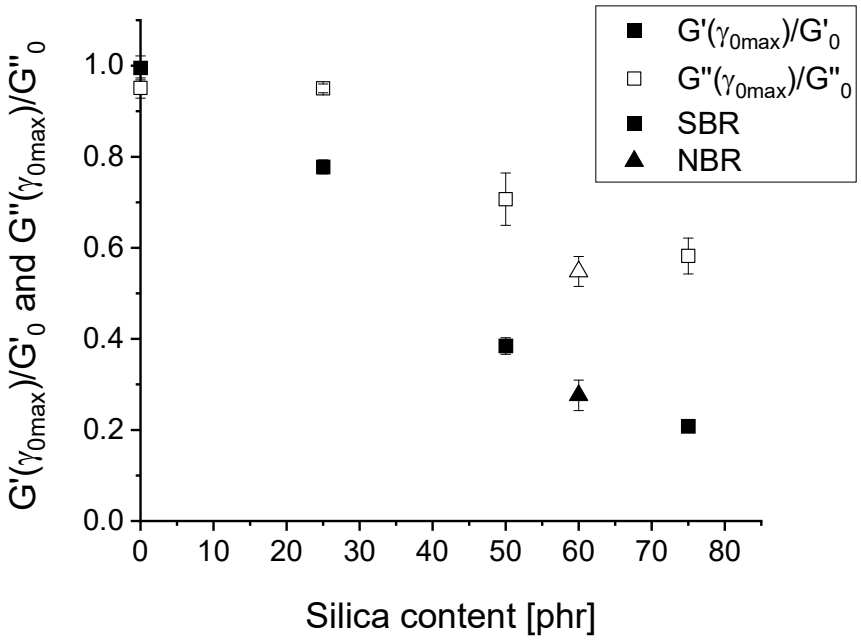

Figure 3.58. The storage (full symbols) and the loss (empty symbols) moduli ratio (eq.1.10) and averaged across the frequencies, in function of the silica content

By looking at the graph, the correlation between the extent of softening, attributed to the Payne effect, and the amount of filler is evident. This correlation can be explained by the increased interconnectedness of the network formed between the particles and the matrix as filler content rises. As a result, there is a greater probability of chain desorption with higher filler concentrations.

4 Conclusion and future developments

Conducting a variety of oscillatory sinusoidal shear tests with a torsional geometry tool on the Anton Paar MCR502 Rheometer, this research shows the impact of time, amplitude, and frequency on the Payne effect observed in silica filled SBR and NBR rubbers. The key findings and issues are listed in the following.

The silica the reinforcing effect and the non-linear response under increasing amplitudes observed on the materials considered in this work are in accordance with literature findings.

The complex modulus dependence on shear strain amplitude is an indication of a no - linear behavior, however, if non-linearity is estimated by a FFT analysis of the shear stress oscillatory response in terms of relative contribution of higher harmonics to the overall response, this is less than 8% respect to the first harmonic. This value is limited enough to allow a data interpretation based on the linear viscoelastic analysis, and G' and G'' can still be considered as valid parameters.

From the series of amplitude sweeps is shown that, for rest times in the order of tens of seconds, the amplitude sweep induces the following changes on the subsequent Payne effect curve respect to the virgin response:

- A significant residual softening of the storage modulus and a small increase of the loss modulus at low amplitudes (in accordance with literature)
- The G' curve displays second plateau at high amplitudes contrary to the virgin curve (sweep #0)

The second point should be further investigated to be sure that this second plateau is not just apparent due to the memory of the material. A possible testing procedure is discussed in the thesis.

Because the ratios between the moduli at low amplitude taken from the sweep #2 and sweep #1 are very close to the unity for all silica contents, it can be stated that the structure, which has been modified by the first amplitude sweep, has no further modifications induced by the subsequent amplitude sweeps. Thus, in other terms, there is no evidence of damage accumulation regardless of the filler content.

The reversibility of the structural modification imposed by the high strain amplitudes is shown by the recovery tests: independently on the silica content, it's demonstrated that if sufficient rest time is waited the reduction of the low amplitude G' would be

completely recovered, even though the recovery kinetic is slow. For the highest silica filled materials, SBR 50 and SBR 75 the recovery time is less than one month.

The structural variations caused by the Payne effect seem therefore to have a reversible nature. Any potential irreversible small changes, if present, do not seem to affect the Payne effect curve after recovery.

Finally, all the observations are mostly independent from the applied frequency: indeed frequency and amplitude seem to have independent effect of the Payne effect curve at higher frequencies (5 – 10 – 20 rad/s). At lower frequencies (0,1 – 1 rad/s) some combined effect seem to be present, however, this may be related again to recovery of the pristine structure occurring during the test, as for these low frequencies recovery times may be comparable to the period of oscillation.

Bibliography

[1] J. Ciambella, Experimental Testing and Nonlinear Viscoelastic Modeling of Filled Rubber, Roma, 2010.

[2] B. Erman, J. E. Mark and C. M. Roland, The Science and Technology of Rubber, Oxford: Elsevier, 2013.

[3] W. D. Callister, Materials Science and Engineering, John Wiley & Sons, 2007.

[4] S. Turri, Principles of polymer chemistry, 2016.

[5] F. Bueche, "Molecular basis for the mullins effect," *Applied Polymer,* vol. 4, no. 10, pp. 107-114, 1960.

[6] F. Bueche, "Mullins effect and rubber-filler interaction," *Applied Polymer,* vol. 5, no. 15, pp. 2771-281, 1961.

[7] S. Wolff, in *International Rubber Conferences*, 1975.

[8] S. Wolff, "Kautsch," *Gummi Kunstst,* vol. 34, p. 280, 1981.

[9] EP501227 and R. Rauline, "Rubber compound and tires based on such a compound," 1991.

[10] WO9928376, E. Custodero, L. Simonot and J.-C. Tardivat, "Reinforcing alumious filler and rubber composition comprising such a filler," 1997.

[11] EP0810258, E. Custodero and J.-C. Tardivat, "Diene rubber composition containing alumina as reinforcing filler and use in tire treads," 1996.

[12] EP1114092, E. Custodero, L. Simonot and J.-C. Tardivat, "Rubber composition for tyre, based on diene elastomer and a reinforcing titanium oxide," 1999.

[13] WO2002053634, L. Simonot, T. Chartier and E. Custodero, "Rubber composition made with diene elastomer and a reinforcing silicon carbide," 2002.

[14] WO2004003067, L. Simonot, A. Lapra, A. Veyland and E. Custodero, "Rubber composition based on diene elastomer and a reinforcing silicon nitride," 2002.

[15] A. P. Legrand, N. Lecomte, A. Vidal, B. Haidar and E. Papirer, "Application of NMR spectroscopy to the characterization of elastomer/filler interactions," *Journal of Applied Polymer Science,* vol. 46(12), p. 2223–2232 , 1992.

[16] J. O'Brien, E. Cashell, G. E. Wardell and V. J. McBrierty, "An NMR Investigation of the Interaction between Carbon Black and cis-Polybutadiene," *Macromolecules,* vol. 9, no. 4, pp. 653-660, 1976.

[17] V. McBrierty and J. Kenny, "Kautsch," *Gummi Kunstst,* vol. 47, p. 342, 1994.

[18] T. A. Vilgis and G. Heinrich, "Disorder-Induced Enhancement of Polymer Adsorption - A Model for the Rubber-Polymer Interaction in Filled Rubbers," *Macromolecules,* vol. 27, no. 26, pp. 7846-7854, 1994.

[19] K. Sone, *International Polymer Science and Technology,* p. 60, 1999.

[20] A. Medalia and G. Kraus, "Reinforcement of Elastomers by Particulate Fillers," *Science and Technology of Rubber (Second Edition),* pp. 387-418, 1994.

[21] F. Bomo, "Influence of a filler such as silica on network formation of elastomers," *Makromolekulare Chemie. Macromolecular Symposia,* vol. 23, no. 1, pp. 321-328, 1989.

[22] H.-G. Kilian, H. Schenk and S. Wolff, "Large deformation in filled networks of different architecture and its interpretation in terms of the van der Waals network model," *Colloid and Polymer Science,* vol. 265, p. 410–423, 1987.

[23] H. Hommel, A. Touhami, A. Legrand and E. P. H. Balard, "Segmental Mobility of Model Compounds for Rubber Reinforcement," *Die Makromolekulare Chemie,* vol. 194, p. 879, 1993.

[24] L. Huang, F. Yu, Y. Liu, A. Lu, Z. Song, W. Liu, Y. Xiong, H. He, S. Li, X. Zhao, S. Cui and C. Zhu, "Structural analyses of the bound rubber in silica-filled silicone rubber nanocomposites reveal mechanisms of filler-rubber interaction," *Composites Science and Technology,* vol. 233, 2023.

[25] J. Diani, B. Fayolle and P. Gilormini, "A review on the Mullins effect," *European Polymer Journal,* vol. 45, p. 601–612, 2009.

[26] Rheometrics System Analyzer RSAIII user manual, 2005.

[27] TA Instruments, Rheology Theory and Applications.

[28] M. Rizza, "Payne effect measurements in simple shear loading conditions," 2020.

[29] L. Chazeau, J. D. Brown, L. C. Yanko and S. S. Sternstein, "Modulus Recovery Kinetics and Other Insights Into the Payne Effect for Filled Elastomers," Center for Composite Materials and Structures Rensselaer Polytechnic Institute, Troy, New York, 2000.

[30] S. Li, Y. Mi and X. Wang, "Superposed nonlinear rheological behavior in filled elastomers," *Journal of Rheology,* vol. 61, no. 3, pp. 409-425, 2017.

[31] X. Fan, H. Xu and C. Wu, "Influences of chemical crosslinking, physical associating, and filler filling on nonlinear," *Journal of Rheology,* vol. 64, p. 775, 2020.

[32] W. Xiong and X. Wang, "Nonlinear responses of carbon black-filled polymer solutions to forced oscillatory shear," *Journal of Non-Newtonian Fluid Mechanics,* vol. 282, 2020.

[33] C. G. R. Amy M Randall, "Linear-nonlinear dichotomy of the rheological response of particle-filled polymers," *Journal of Applied Polymer Science,* vol. 131, no. 19, 2014.

[34] C. Dessi, S. Coppola and D. Vlassopoulos, "Dynamic mechanical analysis with torsional rectangular geometry: A critical assessment of constrained warping models," *Journal of Rheology,* vol. 65, no. 3, pp. 325-335, 2021.

[35] C. Dessi, G. D. Tsibidis, D. Vlassopoulos and M. D. Corato, "Analysis of dynamic mechanical response in torsion," *Journal of Rheology,* vol. 60, no. 2, p. 275, 2016.

[36] L. Di Giosa, "Dynamic Mechanical Analysis in torsion on silica-filled styrene-butadiene rubber," 2022.

[37] W. P. Fletcher and A. N. Gent, "Non-Linearity in the Dynamic Properties of Vulcanised Rubber Compounds," *Trans. Inst. Rubber Ind.* , vol. 29, p. 266–280, 1953.

[38] A. R. Payne, "The dynamic properties of carbon black-loaded natural rubber vulcanizates. Part I," *Journal of Applied Polymer Science,* vol. 6, no. 19, pp. 57-63, 1962.

[39] C. G. Robertson and X. Wang, "Spectral hole burning to probe the nature of unjamming (Payne effect) in particle-filled elastomers," *Europhys. Lett.*, vol. 76, no. 2, pp. 278-284, 2006.

[40] E. Dannenberg, *Trans. Inst. Rubber Ind.*, vol. 42, no. T26, 1996.

[41] S. N. Ganeriwala and C. A. Rotz, "Fourier transform mechanical analysis for determining the nonlinear viscoelastic properties of polymers," *Polymer Engineering & Science*, vol. 27, no. 2, pp. 165-178, 1987.

[42] M. Wilhelm, "Fourier-Transform Rheology," *Macromolecular Materials and Engineering*, vol. 287, no. 2, pp. 83-105, 2002.

[43] J. Dealy and K. Wissbrun, Melt Rheology and Its Role in Plastics Processing: Theory and Applications, 1990.

[44] R. H. Ewoldt, A. E. Hosoi and G. H. McKinley, "New measures for characterizing nonlinear viscoelasticity in large amplitude oscillatory shear," *The Society of Rheology*, vol. 52, p. 1427, 2008.

[45] S. Rogers, "Large amplitude oscillatory shear: Simple to describe, hard to interpret," *American Institute of Physics*, vol. 71, no. 7, p. 34, 2018.

[46] B. M. Erwin, S. A. Rogers, M. Cloitre and D. Vlassopoulos, "Examining the validity of strain-rate frequency superposition when measuring the linear viscoelastic properties of soft materials," *Journal of Rheology*, vol. 54, no. 2, pp. 187-195, 2010.

[47] S. Gupta, S. K. Kundu, J. Stellbrink, L. Willner, J. Allgaier and D. Richter, "Advanced rheological characterization of soft colloidal model systems," *Journal of Physics: Condensed Matter*, vol. 24, no. 46, 2012.

[48] T. S. K. Ng and G. M. R. Ewoldt, "Large amplitude oscillatory shear flow of gluten dough: A model power-law gel," *Journal of Rheology*, vol. 52, no. 2, pp. 417-449, 2008.

[49] G. Heinrich and M. Klüppel, "Recent Advances in the Theory of Filler Networking in Elastomers," in *Filled Elastomers Drug Delivery Systems* , 2002, pp. 1-44.

[50] J. L. Leblanc, "Large amplitude oscillatory shear experiments to investigate the nonlinear viscoelastic properties of highly loaded carbon black rubber

compounds without curatives," *Journal of Applied Polymer Science,* vol. 1090, no. 2, pp. 1271-1293, 2008.

[51] M. Rendek and A. Lion, "Strain induced transient effects of filler reinforced elastomers with respect to the Payne Effect: expirements and constitutive modelling," *ZAMM,* vol. 90, no. 5, pp. 436-458, 2010.

[52] J. A. C. Hardwood and A. R. Payne., *J. Appl. Polym. Sci.,* vol. 10, no. 315-324, 1966.

[53] P. G. Joshi and A. I. Leonov, "Modeling of steady and time-dependent responses in filled, uncured, and crosslinked rubbers," *Rheologica Acta volume,* vol. 40, p. 350–365, 2001.

[54] L. Jong, "Effect of soy spent flakes and carbon black co-filler in rubber composites," *Composites Part A: Applied Science and Manufacturing,* vol. 38, no. 2, pp. 252-264, 2007.

[55] N. R. T. L. Mullins, "Stress softening in rubber vulcanizates. Part I. Use of a strain amplification factor to describe the elastic behavior of filler-reinforced vulcanized rubber," *Journal of Applied Polymer Science,* vol. 9, no. 9, pp. 2993-3009, 1965.

[56] A. R. Payne, *Journal of Applied Polymer Science,* vol. 8, pp. 2661-2686, 1965.

[57] A. R. Payne, "Hysteresis in rubber vulcanizates," *Journal of Polymer Science: Polymer Symposia,* vol. 48, no. 1, pp. 169-196, 1974.

[58] G. Kraus, "Mechanical losses in carbon-black-filled rubbers," *J Appl Polym Sci, Appl Polym Symp,* vol. 39, pp. 75-92, 1984.

[59] X. Wang and C. G. Robertson, "Strain-induced nonlinearity of filled rubbers," *Phys. Rev. E,* vol. 72, no. 3, 2005.

[60] G. Huber, T. A. Vilgis and G. Heinrich, "Universal properties in the dynamical deformation of filled rubbers," *Journal of Physics: Condensed Matter,* vol. 8, pp. L409-L412, 1996.

[61] X. Wang and C. G. Robertson, "A new spectral memory of filled rubbers," *Journal of Polymer Science Part B: Polymer Physics,* vol. 48, no. 8, pp. 859-869, 2010.

[62] A. Franck, "Evaluation of the correct Modulus in Rectangular Torsion".*TA Instruments.*

A Selection of the rest time parameter

This chapter delves into the rationale behind selecting rest time values for the series of amplitude sweeps. These parameters are influenced by the material type and the frequency used in the amplitude sweep. It was observed that if the rest time is too brief, the material's recovery effect might occur during the amplitude sweep, leading to a non-linear behavior in the low amplitude region of the G' and G'' curves (Figure 3.20). Because the recovery kinetics of all materials studied slow down over time, the rest time is designed to allow sufficient recovery, minimizing its impact on the initial points of the moduli.

An additional complexity is that amplitude sweeps performed at different frequencies have varying test velocities. In other terms sweeps at higher frequencies are completed more quickly, resulting in less time for recovery and, consequently, a need for shorter minimum rest times.

Based on these concepts, the subsequent Table A.1 presents the set of rest time values employed in the series of amplitude sweeps (Section 2.2.4) for all frequencies and materials used. It's crucial to emphasize that these values are empirically determined and serve merely as an indication of the minimum rest time required.

Table A.1. List of minimum rest time values in seconds [s] as function of the chosen frequency and the material

Frequencies [rad/s]	SBR 0	SBR 25	SBR 50	SBR 75	NBR 60
0.1	/	300	/	300	250
1	6	150	/	/	/
5	6	30	120	120	70
10	6	25	110	120	/
20	6	20	55	65	60

List of Figures

List of Tables